Contents lists available at ScienceDirect

# **Applied Materials Today**

journal homepage: www.elsevier.com/locate/apmt



# Bio-composite design and 3D printing of soft multi-functional meta-structures with tuneable quasi-constant force

K. Rahmani <sup>a</sup>, H. Malekmohammadi <sup>a</sup>, A.M. Haque <sup>b</sup>, S. Karmel <sup>c</sup>, C. Branfoot <sup>d</sup>, I. Pande <sup>e</sup>, P. Breedon <sup>a</sup>, M. Bodaghi <sup>a,\*</sup>

- <sup>a</sup> Department of Engineering, School of Science and Technology, Nottingham Trent University, Nottingham, NG11 8NS, UK
- <sup>b</sup> Advanced Manufacturing Research Centre (AMRC), Rotherham, S60 5TZ, UK
- Rheon Labs, London, SW8 3QJ, UK
- <sup>d</sup> Engineering Operations, National Composites Centre, Bristol, BS16 7FS, UK
- <sup>e</sup> Rheumatology Department, Queen's Medical Centre, Nottingham University Hospitals NHS Trust, Nottingham, NG7 2UH, UK

#### ARTICLE INFO

# Keywords: Thermoplastic polyurethane Bamboo charcoal Carbon nanotubes Quasi-zero stiffness Finite element modelling Metamaterials

#### ABSTRACT

This study presents a novel, 3D printable, multifunctional bio-composite material system for quasi-zero stiffness (QZS) mechanical metamaterials, transitioning from material development to structural implementation. Biobased thermoplastic polyurethane (TPU) is reinforced with 3-5 wt.% bamboo charcoal (BC), 1 wt.% carbon nanotubes (CNT), and extruded for 3D printing via fused filament fabrication (FFF). The newly developed biocomposite shows up to 86 % strength enhancement and 35 % reduction in flammability. A surrogate-based optimisation method is implemented to calibrate a second-order Ogden hyper-elastic model using tensile data, enabling accurate prediction of nonlinear mechanical behaviours. Inspired by the human ribcage, QZS metastructures were designed with dual-arched geometries and fabricated using the optimised TPU/BC/CNT composite. A finite element model is developed to digitally design the meta-structure and carry out a parametric study. Experimental and computational analyses demonstrate a materially tuneable constant-force plateau (e.g., 2.3-5.12 N) extending across a 6 mm displacement range, with excellent agreement between FEM and test results. Notably, the composite-based QZS structures show an 88 % increase in cyclic energy dissipation versus pure TPU. This response exhibits only limited early-cycle Mullins-type softening that stabilises by 10 cycles, retains 98 % of the maximum force at 1000 cycles, and remains durable under repeated loading-unloading. A modular triple-unit configuration further triples the force capacity without compromising QZS behaviour. This material-to-structure integration provides a scalable, sustainable pathway for engineering adaptive, load-bearing systems applicable to soft robotics, automotive interiors, and protective medical devices where force regulation, overload protection, safety, and comfort are desired.

## 1. Introduction

Mechanical metamaterials, engineered architectures exhibiting unconventional mechanical behaviours, have gained significant attention due to their unique functionalities, such as negative Poisson's ratio (auxeticity) [1], negative stiffness [2], phononic bandgaps [3], and quasi-zero stiffness (QZS) characteristics [4]. These properties enable tailored performance in applications ranging from impact reduction and vibration isolation to energy absorption and adaptive load-bearing systems [5–8]. Among these, QZS metamaterials stand out for their ability to deliver a nearly constant reaction force over a range of displacements.

This makes them highly suitable for energy absorption/dissipation, overload protection, and low-frequency vibration isolation in fields like aerospace, robotics, and wearable devices [9,10].

QZS behaviour typically results from the meticulous design of internal geometries that balance positive and negative stiffness elements within the structure [11]. QZS metamaterials with programmable multi-stability have shown great potential for adaptive systems and multi-functional applications due to their tuneable mechanical responses [12]. Early studies, such as those by Carrella et al. [11], laid the groundwork for QZS design by analysing transmissibility in nonlinear vibration isolators. More recent innovations have taken inspiration from

E-mail address: mahdi.bodaghi@ntu.ac.uk (M. Bodaghi).

<sup>\*</sup> Corresponding author.

biological systems to enhance energy absorption and mechanical adaptability. Sun et al. [13] developed a knee-inspired isolation structure, while Liu et al. [14] explored origami-based QZS metamaterials with multidirectional capabilities. Notably, Hamzehei et al. [15] provided a comprehensive review of QZS mechanical metamaterials for passive vibration isolation, offering design strategies that encompass various architectures. The review emphasised theoretical frameworks over empirical scalability assessments. Ji et al. [16] also critically examined metamaterials and origami structures for vibration control, highlighting abnormal elastic constants in auxetic, band gap, as well as origami's nonlinear stiffness and multi-stability. The review noted challenges in fabrication and dynamic modelling, suggesting future interdisciplinary integration. The integration of negative stiffness elements further improved isolation performance and responsiveness. Additive manufacturing techniques, such as 3D and 4D printing, have further expanded design freedom, enabling the fabrication of geometrically complex, tuneable, and adaptive QZS metamaterials [17,18]. For instance, Zhou et al. [17] demonstrated bio-inspired 4D-printed polygonal structures with adaptive stiffness. Bodaghi et al. [18] 4D printed shape-memory metamaterials with an auxetic combination of soft-hard materials for stiffness tuneability. Recent studies have proposed, for example, origami-based [19] and coral-inspired [20] metamaterials with single- and multi-stability features, utilising variable stiffness characteristics to tune vibration-isolation and QZS performance. In addition to the meticulous design by balancing negative and positive stiffness elements to achieve QZS, other methods such as topology optimization can also be used to design QZS meta-structures. Lu et al. [21] introduced topology optimisation to develop QZS meta-structures, achieving approximately constant stiffness (e.g., 0.502 N/mm over 17 mm) without pre-defined components. Xu et al. [22] proposed programmable QZS designs with smooth boundaries, enhancing stability and broad isolation frequency ranges, validated through nonlinear finite element analysis and experiments.

Hyper-elastic materials, including rubbers, elastomers, and biological tissues, exhibit inherent nonlinear stress-strain behaviours under moderate to large deformations. Hyper-elastic polymers are usually used to design QZS structures with large strain tolerance and recoverable deformations. Thermoplastic polyurethane (TPU) is one such material, offering high elasticity, durability, and excellent processability for 3D printing [23,24]. However, TPU's relatively low mechanical strength and flammability limit its use in designing metamaterials with force level tuneability for real-world applications. Incorporating functional fillers such as carbon nanotubes (CNTs) into TPU matrix was proposed to enhance their mechanical and thermal properties. For example, Rigotti et al. [24] showed that TPU/CNT composites offer improved thermal conductivity and multifunctionality, while Khan et al. [25] used CNTs to tune mechanical stiffness. Recently Bamboo Charcoal (BC) has been proposed a bio-additive to reinforce polymers like polylactic acid and TPU and enhance their flame retardancy [26,27]. Using bamboo charcoal as a renewable, bio-based material reduces petroleum-based fillers and lowers the composite's carbon footprint. This circular approach not only improves flame resistance and strength but also supports sustainability and reduces waste. Therefore, the synergistic effect of CNT and BC in TPU matrix is hypothesised to be promising for developing high-performance, multi-functional hyper-elastics.

Despite these advancements, several critical research gaps and salient limitations remain unaddressed in the field of QZS metamaterials, more specifically, around soft and flexible (e.g., TPU-based) metamaterials. First, while TPU and its composites have been widely explored for general mechanical reinforcement, their performance in QZS applications particularly in terms of achieving tuneable force levels and durability, has not been systematically studied. Current designs achieve QZS only over a narrow displacement range and short plateau regions and often rely on preload or auxiliary loads. Second, the synergistic influence of hybrid fillers such as BC and CNT on the nonlinear hyper-elastic behaviour of TPU within QZS architectures and hysteretic

energy dissipation remains unexplored. Moreover, hysteresis and energy dissipation are often poorly controlled, especially in soft polymer systems. Third, there is a lack of an accurate, experimentally validated hyper-elastic finite element model (FEM) for a multi-phase TPU/BC/CNT composite and its meta-structures. Traditional parameter identification for hyper-elastic models typically relies on computationally intensive trial-error FEMs. Fourth, no study has integrated material characterisation, hyper-elastic modelling, and structural-level QZS performance analysis into a single workflow. Existing research often focuses either on material-level properties [28] or on structural behaviours [29] with very limited emphasis on linking the two through predictive computational models supported by experimental validation.

This study addresses these gaps by developing novel, multifunctional TPU-based bio-composites, reinforced with 0, 3, 5 wt. % BC, and 1 wt. % CNT, and meta-structures with QZS features. The research as depicted in Fig. 1 follows a comprehensive material-tostructure workflow including bio-composite material preparation, hyper-elastic modelling along with surrogate-based calibration, filament extrusion, 3D printing, conceptual design of QZS meta-structures, parametric studies, and finally experimental validation. Biocomposites were developed and extruded for filament fabrication followed by Fused Filament Fabrication (FFF) 3D printing. An array of thermo-mechanical experiments reveals their improved stiffness, mechanical properties and flame retardancy with an acceptable extrudability. The hyper-elastic constitutive Ogden model was implemented to replicate the material behaviours. Tensile testing results were used to calibrate the constitutive model. An autonomous calibration was developed by implementing an efficient surrogate-based optimisation process. Inspired by the human ribcage, QZS metamaterials were designed as dual-arched (concave/convex) unit cells. The ribcage's segmented, multi-rib architecture with semi-flexible joints provides flexibility, adaptability, and load sharing, yielding distributed energy dissipation and a low incremental stiffness region around the neutral breathing posture. These could be mapped directly onto QZS requirements: a near-constant reaction force over a finite stroke, programmable multi-stability, and tunability via geometric parameters. Operationalising this rationale, the design achieves controllable quasiconstant-force plateaus by adjusting curvature radii, inter-arch spacing, thickness, and pre-camber, while remaining compatible with monolithic FFF fabrication in a soft bio-composite. An FEM simulation platform was established based on the Ogden model to predict the mechanical response of the composite at material and meta-structure levels under monotonic loading and cyclic loading-unloading conditions. QZS meta-structures were 3D printed, and their mechanical performance was assessed through quasi-static compression tests via experimental and computational studies. The computational results are in excellent agreement with the experimental force-displacement outputs, confirming the reliability of the material model, the effectiveness of the surrogate-based optimisation approach, and FEM accuracy. The bioinspired meta-structures with arc-shaped components demonstrate stable constant-force behaviours across a 6 mm plateau, tuneable force levels from 2.3 to 5.12 N, and hysteretic energy dissipation with only minor early-cycle softening. The response then stabilises and retains 98 % of the maximum compressive force after 1000 cycles. Additionally, a modular triple-unit configuration was investigated, revealing a tripling of force capacity while preserving the QZS characteristics. By systematically integrating material design, experimental characterisation, computational modelling, and structural validation, this research contributes a significant advancement towards sustainable, highperformance QZS metamaterials suitable for automotive, robotic, and safety/comfort/protective systems.

#### 2. Manufacturing and experimental setup

This research aims to develop novel QZS mechanical metamaterials and study their material composition and structural design. This section

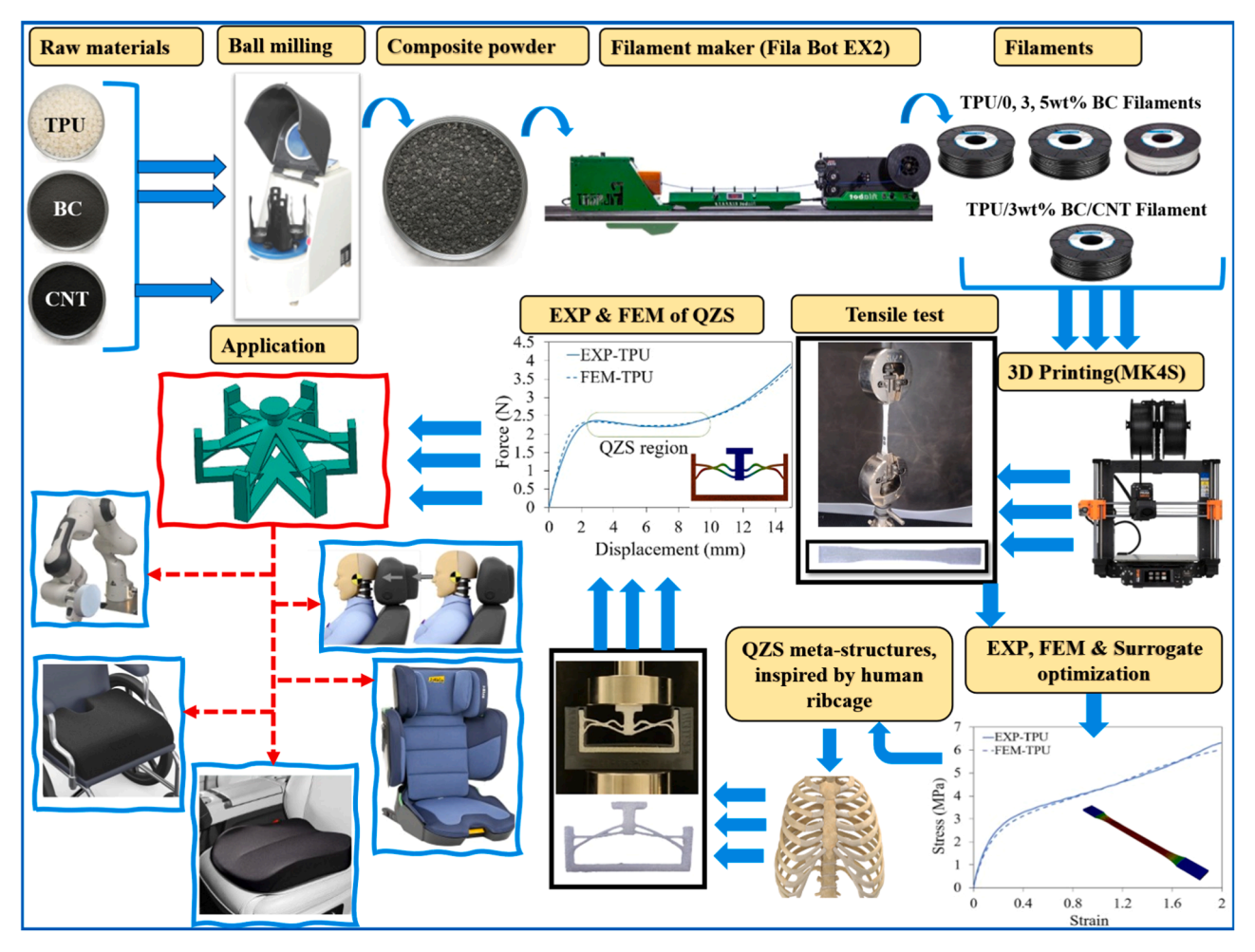


Fig. 1. A workflow of processes for creating TPU/BC/CNT bio-composite, covering the stages from raw materials to testing and exploring potential applications.

explains the materials used to reinforce the new bio-composite and describes the manufacturing steps and experimental testing methods.

#### 2.1. Raw materials

This research introduces an innovative bio-composite material system designed for additive manufacturing of QZS mechanical metamaterials. The developed bio-composite demonstrates several desirable properties, including enhanced mechanical strength, efficient energy dissipation, flame retardancy, and biocompatibility [27]. Bio-based TPU pellets (Nanovia, France, shore hardness: 93A), as shown in Fig. 2, were selected as the base material due to their excellent flexibility for applications involving large deformations. The bio-based Nanovia TPU also offers advantages such as biodegradability, recyclability, renewable sustainability, and moisture resistance, though it is limited by relatively low mechanical strength and flammability. To address this limitation, CNT powder (Merck, USA) plus BC powder (Takesumi Ltd., Japan) as a natural, plant-based reinforcement were incorporated into the TPU matrix. These additives were expected to significantly improve the mechanical performance, structural integrity, and flame retardancy of the TPU-based bio-composites.

# 2.2. Bio-composite filament development

The flowchart in Fig. 2 presents the process by which the biocomposites were produced. Initially the raw materials of TPU pellets, BC powder, and CNT powder were procured. The production of the biocomposite went through three distinct but sequential steps: (i) TPU

pellets and BC and CNT powders ball milling to achieve a homogeneous mixture, (ii) extruding the composite filament, and (iii) 3D printing the TPU bio-composite filaments. Representative images of the filaments production step of TPU, TPU/BC and TPU/BC/CNT composites are shown in Fig. 2. In the initial phase, raw TPU granules were subjected to a drying regimen in a laboratory oven at 60 °C for a duration of 6 h to eliminate residual moisture. To produce TPU composites, a set of 0, 3, and 5 wt. % BC, respectively and, another set of 3 wt. % BC and 1 wt. % CNT were separately added to pre-dried TPU granules in a planetary ball mill. CNT was incorporated for its proven ability to enhance the Young's modulus, and the 1 wt. % loading was selected as it provided the most effective improvement [30,31]. A blending time of 10 min was employed to ensure a uniform dispersion of both BC and CNT particles throughout the TPU matrix. Subsequently, the produced TPU/BC and TPU/BC/CNT composites mixtures from the blended process were fed into a filament extruder (Filabot EX2, VT, USA) equipped with a speed-controlled spooler. The extrusion temperature was set to 190  $^{\circ}\text{C}$ for all extruded filaments, producing TPU composites filaments with diameters of 1.75 mm. All specimens were fabricated with Fused filament fabrication (FFF) based 3D printer (Original Prusa MK4S), as outlined in Table 1. TPU filaments and those reinforced with varying weight percentages of BC (0, 3, and 5 wt. %) are denoted as TPU/X wt. % BC, where X represents 0, 3, and 5. Additionally, TPU/3 wt. % BC specimens further reinforced with 1 wt. % CNT are denoted as TPU/3 wt. % BC/CNT, respectively.

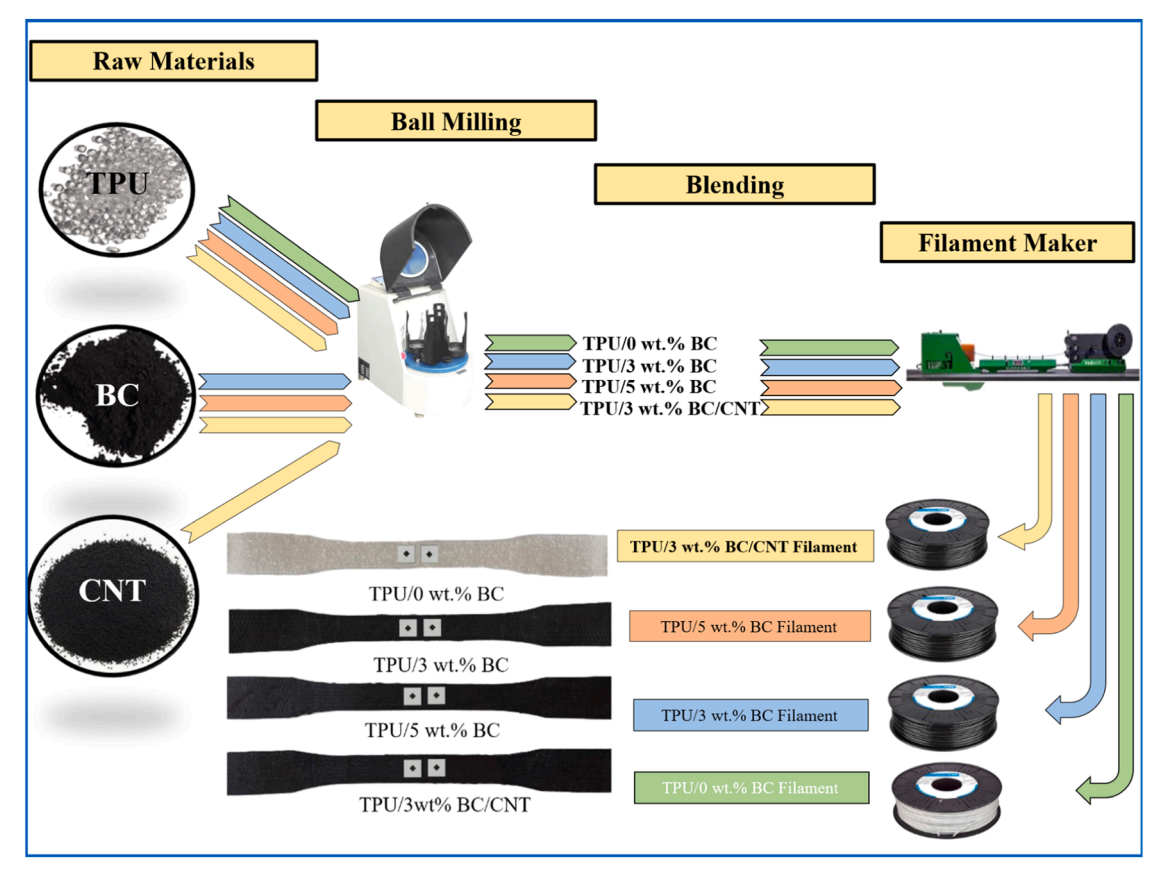


Fig. 2. A process schematic for developing TPU/BC and TPU/BC/CNT bio-composite filaments.

**Table 1**3D printing parameters.

Parameters	Value
Nozzle diameter (mm)	0.4
Layer thickness (mm)	0.2
Printing speed (mm/s)	35
Infill density ( %)	100
Printing pattern	Linear
Nozzle temperature ( °C)	235
Bed temperature ( $^{\circ}C$ )	65

# 2.3. Melt flow index (MFI)

To evaluate the melt processability of the prepared materials, the MFI was determined for pure TPU and its bio-composites incorporating BC and CNT. The experimental procedure adhered to the ASTM ISO 1133 standard, employing a test temperature of 210  $^{\circ}C$  and a standard load of 5 kg. For enhanced statistical reliability, five independent measurements were conducted for each material formulation. The resulting extrudate mass data were averaged to calculate the definitive MFI value, reported in unit of g/10 min.

## 2.4. Dynamic mechanical thermal analysis (DMTA)

Functional performance and structural integrity of 3D-printed polymer composites in different thermal environments depend critically on their thermomechanical properties, especially storage modulus, and glass transition temperature ( $T_g$ ). These properties delineate the composite material's stiffness and changes between a glassy, rigid state and a rubbery and more compliant state. This research specifically examines the thermomechanical properties of pure TPU and TPU matrix reinforced by BC and CNTs. The goal is to reveal the individual and potential

synergistic effects on the thermomechanical properties of the 3D-printed composites. To this end, DMTA was conducted with a PerkinElmer DMTA 8000 analyser. Samples were 3D printed with a dimension of 30 mm (length)  $\times$  8 mm (width)  $\times$  1 mm (thickness). The dynamic mechanical characterisation was completed according to the ASTM D4065 -01 standard in a single cantilever bending mode. The samples underwent a temperature ramp from  $-100\,^{\circ}\mathrm{C}$  to  $+100\,^{\circ}\mathrm{C}$  external temperature at a linear heating rate of 5  $^{\circ}C$  /min. Throughout the thermal cycling, the samples experienced a sinusoidal deformation with a constant frequency of 1 Hz.

# 2.5. Flammability test

Flame resistance is a critical safety attribute for materials utilised in diverse applications where fire hazards are present. The flammability characteristics of the composites were comprehensively investigated through the Underwriters Laboratories (UL-94) horizontal test. The flammability of the samples, specifically their burning rate and duration in a horizontal position, was evaluated consistent with ASTM D635–22 standard. For this evaluation, printed samples were positioned horizontally within a fume hood and marked at 25 mm and 100 mm distances from one end. The time taken for the flame front to propagate from the 25 mm mark to the 100 mm mark, along with the burned length, was recorded. The burning rate (S) of the composites was calculated by multiplying the burned length in millimetres by 60 and dividing by the burning time in seconds.

# 2.6. Mechanical test

The tensile properties of the reinforced bio-composites were assessed using a Shimadzu AG-X Plus machine. For this evaluation, dog-bone samples of ASTM Dd-638 Type I at a speed of 5 mm/min were

prepared for TPU, TPU/BC, and TPU/BC/CNT bio-composites. Five samples were tested for each composite material, with the reported mechanical properties reflecting the average data derived from these results

Specimens of the proposed QZS meta-structures were tested under both monotonic and cyclic compression to evaluate their forcedisplacement and energy dissipation characteristics. For the monotonic compression test, a 15 mm displacement was applied to the top surface of each specimen at a speed of 5 mm/min, with the stiffening walls supported by a printed cage to simulate fixed boundary conditions. In the cyclic test, the specimens were subjected to a compression displacement of 15 mm at the same speed, followed by an unloading phase. It is worth noting that the testing speed in this study was chosen to produce a low strain rate, thereby simulating quasi-static conditions and behaviour. While this approach is valid for many applications, there are also many scenarios in which materials and structures experience high strain rates. Since this research focuses on low strain rate and quasistatic conditions, dynamic loading scenarios involving high strain rates were not considered but could be explored in future work. For more information on dynamic testing and modelling of meta-structures, the reader is referred to [10].

#### 3. Computational modelling

This section presents a new method for computing the constitutive behaviours of bio-composite TPU. The method includes three stages. First, a theoretical formulation was established based on the Ogden hyper-elastic material model that is capable of capturing non-linear mechanical behaviours. Second, FEM was used to predict the response of the material under uniaxial tensile loading, and thus the estimated relationship for stress and strain based on the Ogden material model. To ensure the accuracy and reliability of the computational simulations, a mesh sensitivity analysis was conducted to achieve mesh independence and solution convergence. This process usually involved a maximum of six iterative modifications of the element density, systematically refining the mesh until a stable solution was attained with an error of < 0.5 %. The third stage consisted of an inverse optimisation by using the surrogate-based optimisation method. In this case, the coefficients of the Ogden model were iteratively optimised by minimising the gap between the measured tensile stress-strain by experimental test and the FEM predicted tensile stress-strain curve. The surrogate model was validated by comparing the FEM-predicted stress-strain curves, and generated using the calibrated Ogden model, with experimental data (Fig. 5 & Fig. 11). It therefore ensures that the extracted coefficients describe the mechanical properties of the bio-composite accurately and are able to create a reliable material model for engineering predictive applications.

# 3.1. Hyper-elastic material model

The Ogden model as an established constitutive framework was chosen to predict nonlinear stress-strain behaviours in hyper-elastic materials under large deformations. It uses a strain energy density function defined in terms of the principal stretches. This definition allows the model to capture more complex mechanical responses than simpler models such as Mooney-Rivlin or Neo-Hookean. These simpler models lack the requisite flexibility to account for multi-term strain energy contributions. The general strain energy potential U for the Ogden model is mathematically expressed as [32]:

$$U = \sum_{i=1}^{n} \frac{\mu_i}{\alpha_i} \left( \overline{\lambda}_1^{a_i} + \overline{\lambda}_2^{a_i} + \overline{\lambda}_3^{a_i} - 3 \right) \tag{1}$$

where  $\lambda_1$ ,  $\lambda_2$ , and  $\lambda_3$  represent the normalised principal stretches,  $\mu_i$  denotes the shear moduli, and  $\alpha_i$  are non-dimensional shape parameters governing the strain hardening/softening behaviour. The number of terms, n, in the summation dictates the model's complexity. A second-

order Ogden model (n=2) is frequently chosen for its balanced accuracy and computational efficiency. In this study, a second-order Ogden model was selected to characterise the material response, aligning with prior validations of its effectiveness in capturing nonlinear deformations within additive manufacturing applications.

#### 3.2. Finite element modelling

A high-fidelity FEM simulation of the tensile test was performed using Abaqus/CAE 2022. The primary objective of this simulation was an experimental validation of the Ogden hyper-elastic material model. This validation was achieved by determining the model's constitutive coefficients and comparing these against quasi-static tensile test data. A three-dimensional solid mechanics model was constructed, employing C3D8RH hexahedral elements. These elements were selected for their balance of accuracy and computational efficiency in simulating large deformations. To ensure mesh independence and solution convergence, a mesh sensitivity analysis was conducted. This involved iteratively refining the element density until convergence was confirmed at a final mesh density of 298,000 elements, deemed sufficient to minimise discretisation errors while maintaining computational tractability. The simulation adopted displacement-controlled boundary conditions to replicate ASTM D638-compliant tensile testing. A rigid constraint was applied to the bottom surface of the specimen (fully fixing all degrees of freedom), while the upper surface was coupled to a reference point (RP) to enforce uniaxial displacement conditions (Fig. 3). A vertical displacement of 20 mm was applied to the RP.

#### 3.3. Surrogate-based optimisation method

To determine the hyper-elastic Ogden material coefficients, a surrogate-based optimisation methodology was utilised that incorporated numerical simulation, experimental data, and optimisation. The optimisation framework integrates a radial basis function (RBF) surrogate with particle swarm optimisation (PSO) to minimise the objective function. The objective is the discrepancy between the experimental and FEM stress-strain curves from tensile tests. Initial sample points are generated by Latin Hypercube Sampling (LHS) within the bounds of the Ogden parameters. For each sample, the FEM model is run to evaluate the objective, and a cubic RBF with a linear polynomial tail is then fitted to these data to approximate the response surface (Eqs. (2)-(6)). PSO explores this surrogate by updating particles based on personal and global bests to propose candidate coefficient sets. Each candidate is

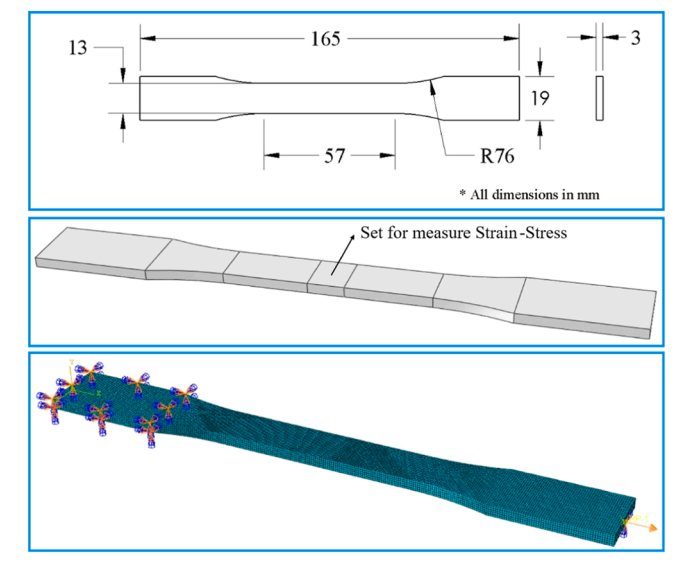
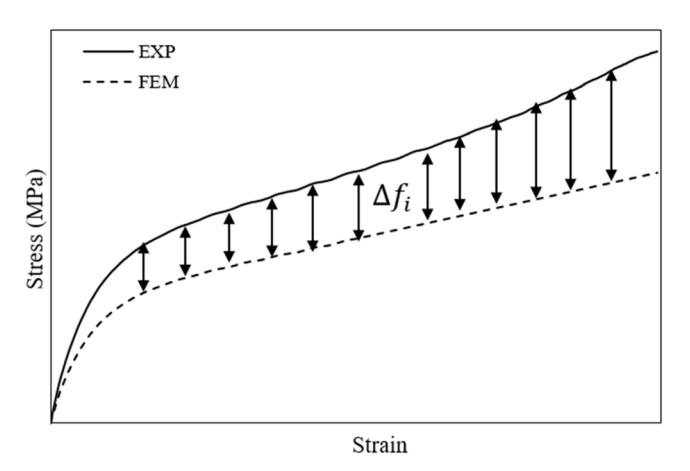


Fig. 3. The finite element modelling of the tensile test.

validated by FEM, the new pairs are appended, and the surrogate is refit iteratively until convergence in the objective is observed.

According to Figs. 4 and 5, the objective function represents the difference between the stress-strain curves obtained experimentally and from FEM. The objective function was minimised using a surrogate modelling process that involved the following iterative steps: 1) design of experiments to create an initial set of data points for simulation; 2) running computational FEM simulations for the selected sample points; 3) developing a surrogate model with the simulation data; 4) executing optimisation of the surrogate to determine new candidate sample points; and 5) iterating through steps 2–4 until convergence. A work-flow of the calibration process is displayed in Fig. 4.

More precisely, step (1) was performed using LHS to initially sample a set of points within the design space. LHS is a statistical technique for space-filling to obtain the maximum pairwise distances between sample points to allow for relatively good coverage of the design space and is especially useful in absence of any prior information. It is important to minimise the number of initial samples to limit the overall computational cost. In step (2), the FEM was executed for each sample point



 $\label{eq:Fig. 5.} \textbf{A} \hspace{0.1cm} \text{comparison} \hspace{0.1cm} \text{of} \hspace{0.1cm} \text{experimental} \hspace{0.1cm} \text{and} \hspace{0.1cm} \text{computational} \hspace{0.1cm} \text{FEM} \hspace{0.1cm} \text{stress-strain} \hspace{0.1cm} \text{curve}.$ 

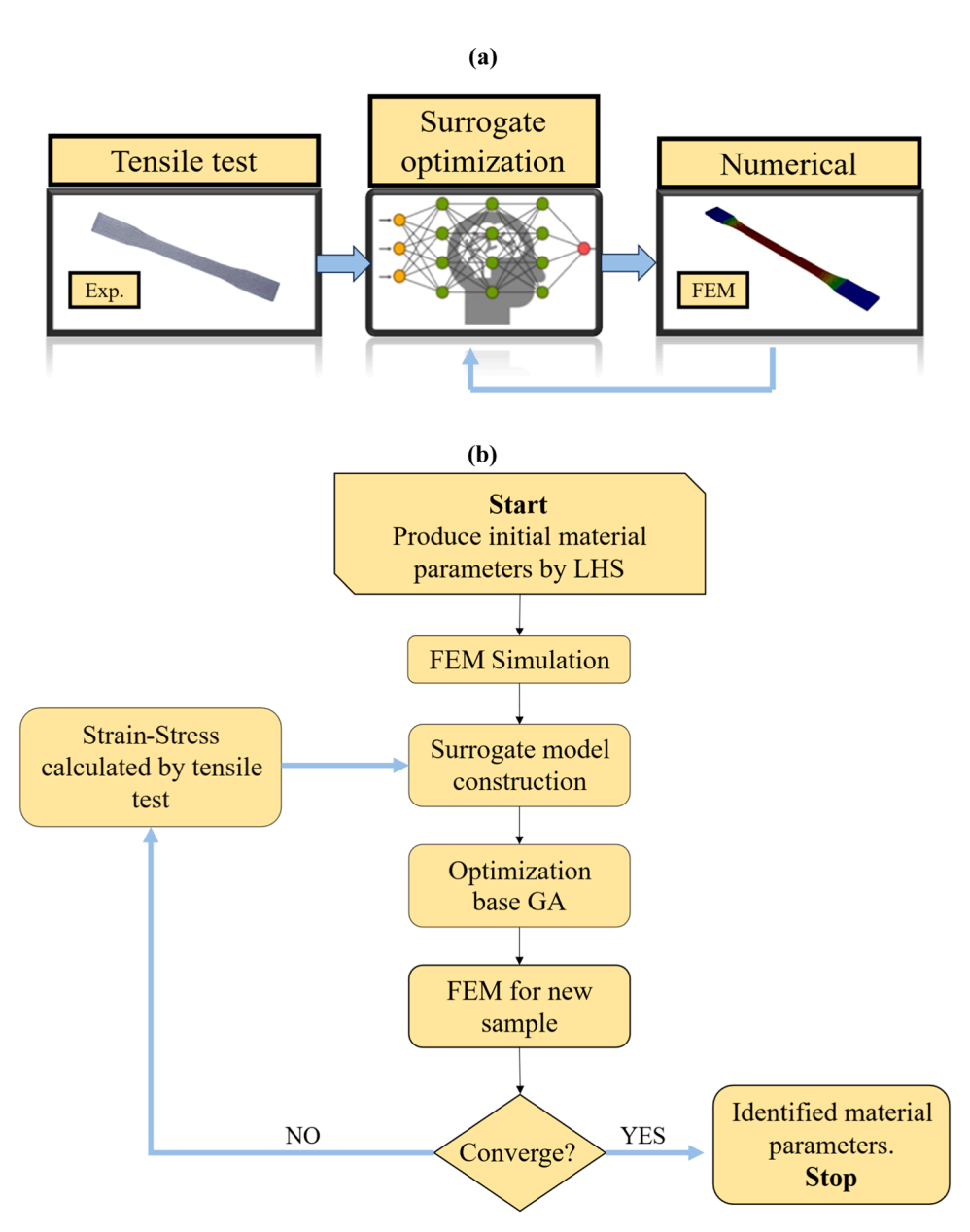


Fig. 4. (a) Optimisation framework and (b) process flow diagram of the inverse method employed for material parameters identification.

generated by the LHS design to obtain the corresponding objective function values. In step (3), a surrogate model, specifically a RBF model, was constructed using the data obtained from the FEM simulations. RBF models approximate the objective function, enabling efficient exploration of the design space. The RBF model, f(x), is defined as:

$$f(x) = \sum_{i=1}^{n} \lambda_{i} f(\|x - x_{i}\|) + p(x)$$
 (2)

where  $\|\|$  denotes the Euclidean norm,  $\lambda_i$  are unknown parameters, p(x) is a linear polynomial function, and f is the radial basis function. In this study, a cubic radial basis function,  $f(r) = r^3$  was employed. The objective function, y(x), within the surrogate model is represented as:

$$y(x) = f(x) + e \tag{3}$$

where f(x) is the approximating function derived from the RBF model, and e represents the random error. If y(x) is considered at the selected points  $x_i = [x^1, x^2, ..., x^n]$  as  $y(x) = [y(x_1), y(x_2), ..., y(x_n)]$ , then the RBF f(x) can be expressed as:

$$f(x) = \sum_{i=1}^{n} \lambda_{i} \phi(\|x - u^{(i)}\|) + p(x)$$
 (4)

This equation can be rewritten in a matrix form as:

$$\begin{bmatrix} \phi & p \\ p^T & 0 \end{bmatrix} \begin{bmatrix} \lambda_i \\ c \end{bmatrix} = \begin{bmatrix} F \\ 0 \end{bmatrix} \tag{5}$$

where  $\phi_{ij} = \phi(\|u^{(i)} - u^{j)}\|)$  and  $i^{th}$  row of matrix p is  $\left[1, \left(u^{(i)}\right)^{T}\right]$ . The vectors  $\lambda_i$ , c, and F are defined as:

$$\lambda_{i} = \begin{bmatrix} \lambda_{1} \\ \lambda_{2} \\ \vdots \\ \lambda_{n} \end{bmatrix}, c = \begin{bmatrix} b_{1} \\ b_{2} \\ \vdots \\ b_{d} \\ a \end{bmatrix}, F = \begin{bmatrix} f(x_{1}) \\ \vdots \\ f(x_{n}) \end{bmatrix}$$

$$(6)$$

in which d depends on the order of the problem.

This study uses the difference between experimental and computational stress-strain curves as the objective function, see Fig. 5. Specifically, n points are selected along the stress-strain curves, and the difference between the experimental and numerical values at each point is calculated using the following equation:

$$\Delta f_1 = |f_1^{exp} - f_1^{num}| \dots \Delta f_n = |f_n^{exp} - f_n^{num}| \tag{7}$$

where the superscripts "exp" and "num" denote experimental and numerical values, respectively. The objective function is then defined as the root mean square of these differences:

$$f(x) = \sqrt{\Delta f_1^2 + \dots + \Delta f_n^2} = \sqrt{\sum_{i=1}^n \Delta f_i^2}$$
 (8)

For the Ogden hyper-elastic model employed in this study, the design space consists of four variables, which are incorporated into the following unknown vector:  $\boldsymbol{x} = [\mu_1, \ \alpha_1, \ \mu_2, \ \alpha_2]$ .

# 4. QZS meta-structure design

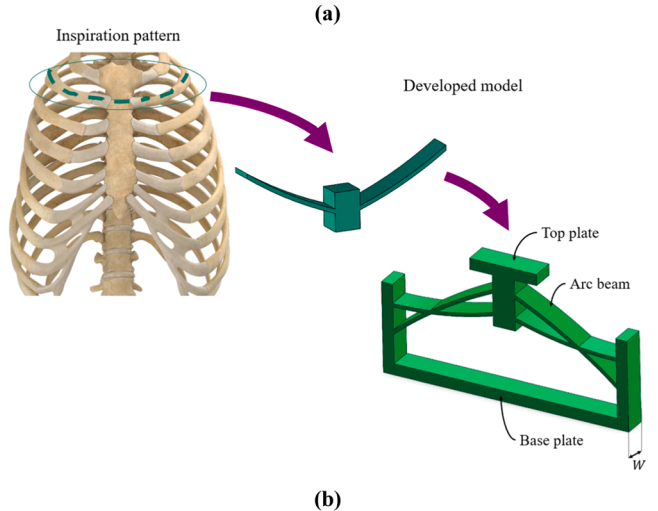
This section investigates the proposed QZS structure through a two-part analysis. Initially, a novel bio-inspired QZS structure is introduced, drawing conceptual elements from human anatomy. Subsequently, the numerical simulation methodology employed to analyse this structure's mechanical response is described.

#### 4.1. Conceptual design

In this study, a novel QZS meta-structure was designed based on two curved beams with concave and convex profiles inspired by the human ribcage. The ribcage features curved ribs that link the spine to the sternum, offering both structural support and flexibility, a mechanism mirrored by the curved beams connecting to the top plate in the proposed design. This biomimetic approach facilitates the development of QZS structures with potential applications in vibration isolation and compliant mechanisms. Its schematic is presented in Fig. 6a. The design consists of three primary components: a U-shape base, hyper-elastic arch beams, and a top plate. Also, Fig. 6b shows the hyper-elastic beam defined by a radius ( $R_1$  or  $R_2$ ) and an angle ( $\theta_1$  or  $\theta_2$ ). For each beam, the angle and radius are adjusted to ensure that the arch length  $(S_1=R_1\theta_1,$  $S_2=R_2\theta_2$ ) remains constant. The beams possess a thickness (T) 1.6 mm, a width (W) 8 mm and the unit cell has a length L = 100 mm. The concave and convex profiles and their combination are expected to enable tuning stiffness from positive to zero and then negative.

#### 4.2. FEM simulation

The quasi-static mechanical behaviours of the designed metastructures were investigated using FEM in Abaqus. Ten-node hybrid quadratic tetrahedron (C3D10H) elements, suitable for large strain deformations with good convergence, were used for discretisation. Geometric nonlinearity was considered to accurately capture the non-linear buckling behaviour of the arch beams. The Ogden hyper-elastic material



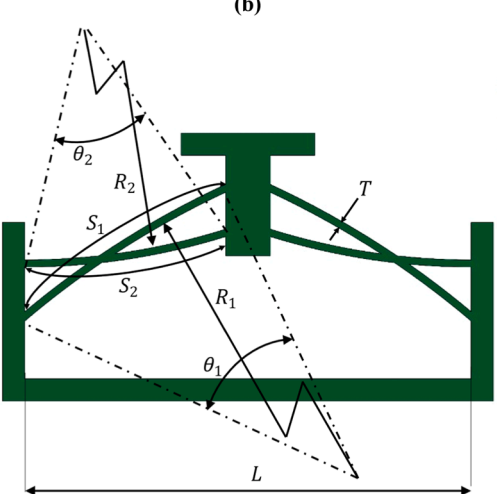


Fig. 6. Schematic diagram of the QZS meta-structure.

model, with parameters derived in the previous section, was implemented as the constitutive model. To simulate the structure's response under load, boundary conditions mimicking the experimental setup were applied. In this respect, the bottom and side surfaces were fully constrained, while the top surface was coupled to a RP. A vertical displacement load was applied to the RP to analyse the quasi-static mechanical behaviour of the meta-structure under compression as shown in Fig. 7. The resulting reaction force-displacement curves at the RP were used to evaluate the QZS response.

#### 5. Results and discussion

# 5.1. MFI of bio-composite TPU

MFI measurements provided quantitative insights into understanding the extrudability feature of the materials. As shown in Fig. 8, the pure TPU exhibits an MFI value of  $19.2\,\mathrm{g}/10\,\mathrm{min}$  under the specified test conditions. Incorporation of BC into the matrix results in a reduction in melt flow, with the TPU/5 wt. % BC composite having an MFI of  $16.3\,\mathrm{g}/10\,\mathrm{min}$ . A further decrease is observed upon the addition of CNTs alongside BC, yielding an MFI of  $13.9\,\mathrm{g}/10\,\mathrm{min}$  for the TPU/3 wt. % BC/CNT formulation. This systematic decrease in MFI signifies an increase in the melt viscosity of the composites compared to TPU. Such behaviour is expected and attributed primarily to the hydrodynamic resistance imposed by the dispersed reinforcement particles (BC and CNTs). They physically obstruct and hinder the cooperative movement and flow of TPU chains within the melt [33,34]. While incorporating BC and CNTs reduces the MFI, TPU/3 wt. % BC/CNT with  $13.9\,\mathrm{g}/10\,\mathrm{min}$  value still shows an acceptable level of extrudability and 3D printability [35].

#### 5.2. DMTA

DMTA was employed to investigate the viscoelastic behaviour and primary thermal transitions of TPU and composites reinforced with BC and CNT. This technique provides crucial information on temperature-dependent stiffness (storage modulus) and damping characteristics (tan $\delta$ ), including the glass transition temperature (Tg). Figs. 9a and 9b illustrate the comparative storage modulus and tan $\delta$  behaviour, respectively, for the pure TPU and composites. Analysis of the storage modulus reveals a significant enhancement in material stiffness for both TPU/BC and TPU/BC/CNT composites compared to pure TPU, particularly evident in the glassy region below Tg. This increase in storage modulus underscores the effective reinforcing role of the BC and CNT particles within the TPU matrix. Concurrently, the tan $\delta$  curves (Fig. 9b), whose prominent peak typically corresponds to the Tg, indicate a subtle but systematic shift in the glass transition. The Tg for pure TPU was determined to be approximately 0 °C, whereas it increases to roughly 3

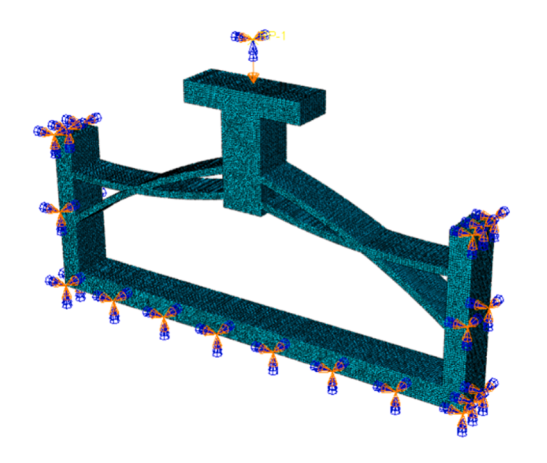


Fig. 7. Finite element modelling of QZS meta-structures with boundary conditions.

 $^{\circ}$ C for TPU/3 wt. % BC and further to 5  $^{\circ}$ C for TPU/3 wt. % BC/CNT composite. Furthermore, the magnitude of the tan $^{\delta}$  peak was notably reduced for the reinforced systems relative to pure TPU. This suppression of the damping peak, coupled with the slight  $T_g$  elevation, suggests a restricted polymer segmental mobility at the reinforcement-matrix interface, indicative of effective interfacial interactions and reduced energy dissipation capacity at the glass transition.

#### 5.3. Flammability properties

The flammability characteristics of bio-composite specimens are quantitatively evaluated employing the UL-94 horizontal burning test. The pure TPU specimens were observed to burn completely, indicating poor flame resistance. Conversely, composites reinforced with TPU/BC and TPU/BC/CNT exhibited incomplete combustion, leaving behind more char. The average burning rate results are presented in Fig. 10. It reveals distinct differences between the samples, substantiating an enhanced flame retardancy via reinforcements. Specifically, the composites demonstrate lower burning rates compared to the pure TPU matrix. It is found that TPU/3 wt. % BC, TPU/5 wt. % BC, and TPU/3 wt. % BC/CNT improve the flame retardancy by 20 %, 27 % and 35 %, respectively, compared to the pure TPU, Notably, TPU/3 wt. % BC/CNT showed better performance than TPU/5 wt. % BC, indicating that CNTs play a role in reducing flammability. CNTs, as shown by Kashiwagi et al. [36], have high thermal stability and help create a protective char layer that slows volatile release, oxygen penetration, and heat transfer. They also strengthen this layer by improving graphitisation, reducing cracks, and connecting the structure, which barriers flame spread. BC supports this process by supplying carbon, while CNTs, with their high aspect ratio and network-forming ability, reinforce the barrier. The combined action of BC and CNTs improves the stability of the protective layer, reduces material degradation, and lowers flame propagation, making TPU/BC/CNT composites promising for sustainable applications that require high fire safety.

#### 5.4. Mechanical behaviour of bio-composites and meta-structures

Fig. 11 demonstrates that the developed FEM analysis based on the computational procedure defined in Section 3 (Computational modelling; see Fig. 4) accurately predicts the mechanical response of the TPU sample, showing a strong agreement with the experimental results. Thus, this calibrated FEM model has been used to simulate the structural behaviour of the meta-bio-composites. It is found that the Ogden model, in conjunction with the surrogate-based calibration method and FEM simulations, adequately replicates the nonlinear hyper-elastic response and softening behaviours of the tested TPU materials in the range of 0–200 % strain. The resulting Ogden material parameters, derived for TPU plus various bio-composite formulations, are presented in Table 2.

The stress-strain curves for various bio-composites are represented in Fig. 12. Distinct mechanical behaviours are observed across different material compositions while the FEM can accurately replicate them all. The polymeric composites incorporating 3 wt. % BC and 5 wt. % BC exhibit noticeable increases in stiffness and tensile strength over the pure TPU, as expected. Specifically, at 200 % strain, the maximum stress observed is 6.3 MPa for pure TPU, increasing to 8.1 MPa for TPU with 3 wt. % BC and 7.5 MPa for TPU with 5 wt. % BC, respectively. This corresponds to a strength enhancement of 28 % for TPU/3 wt. % BC and 19 % for TPU/5 wt. % BC, respectively, compared to pure TPU. The comparatively lower mechanical performance of the TPU/5 wt. % BC composite versus the TPU/3 wt. % BC formulation is potentially attributable to reinforcement agglomeration and clumping at the higher BC concentration. To validate the hypothesis regarding reinforcement agglomeration at higher filler content, SEM analysis was conducted on TPU and TPU bio-composite. As shown in Fig. 12a, the TPU/3 wt. % BC composite and a composite with TPU/3 wt. % BC/CNT exhibit a relatively uniform dispersion of particles, while the TPU/5 wt. % BC sample

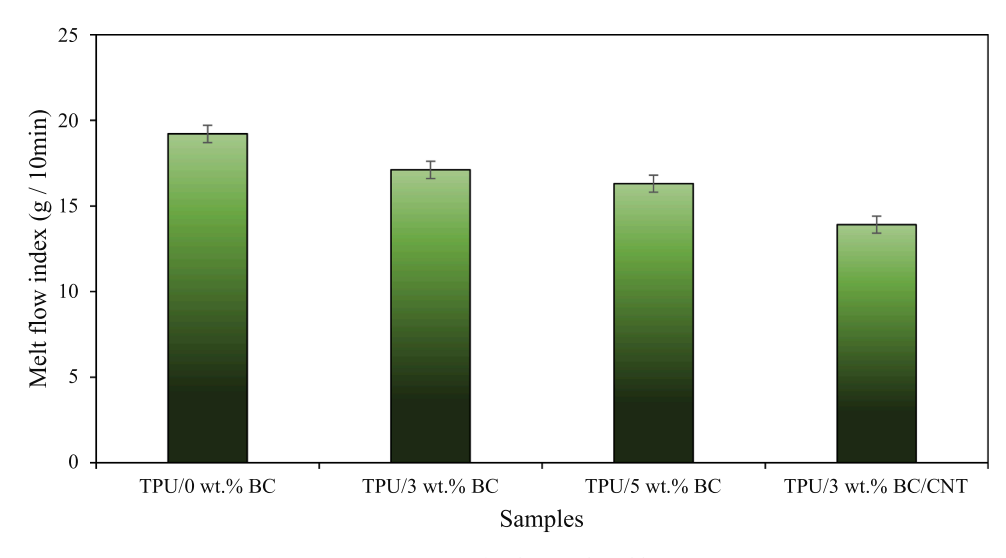


Fig. 8. MFI measurements for the TPU-based bio-composites.

clearly reveals visible agglomerates and clustering of BC particles. This confirms that excessive filler loading compromises dispersion quality. Also, Figs. 12a present the high-magnification SEM images of CNT and BC particles together with their Energy-Dispersive X-ray (EDX) spectra. At high magnification, CNTs appear as entangled fibrils or bundles with a high aspect ratio, whereas BC is observed as irregular microparticles embedded in the TPU matrix. The EDX analysis further confirms the presence of both BC and CNT particles. These findings support the assertion that the reduced mechanical performance at higher BC content is due to particle agglomeration and poor interfacial distribution. Also, it may be attributed to the single-screw extrusion process. Improved dispersion methods, such as twin-screw compounding, are expected to further optimise performance [37].

The most significant enhancement in mechanical properties is observed with the incorporation of CNTs alongside 3 wt. % BC. The TPU/3 wt. % BC/CNT composite exhibits the highest stress values throughout the entire strain range compared to the other systems tested, suggesting a synergistic effect between BC and CNTs [38]. In this formulation, the maximum stress recorded at 200 % strain is 11.7 MPa, representing an 86 % increase in strength when compared to the TPU/3 wt. % BC composite. This pronounced improvement is likely due to the high aspect ratio, fine particle size, uniform distribution, inherent stiffness, and excellent mechanical properties of CNTs. These facilitate efficient stress transfer and reinforcement within the TPU matrix, even at a relatively low CNT content.

Following the material characterisation, a parametric study was conducted to investigate the influence of key geometric parameters on the QZS properties of the meta-structures. Eight parameters (Fig. 6) were defined under given design constraints. The thickness of the arch ( $T=1.6\,$  mm) and span length ( $L=100\,$  mm) were fixed. Since the arch volume is constant, the arch lengths (S1 and S2) also remain constant. This links the radius of curvature ( $\mathbf{R}$ ) and the angle ( $\mathbf{\theta}$ ), because  $S=\mathbf{R}\mathbf{\theta}$ . In the study,  $\mathbf{R}$  and  $\mathbf{\theta}$  were varied while keeping  $\mathbf{S}$  constant. Thus, choosing a radius automatically sets the angle. The main design variables were  $\mathbf{R}\mathbf{1}$  and  $\mathbf{R}\mathbf{2}$ , which control stiffness. The "concave" and "convex" profiles were obtained by orienting the arches inward or outward relative to the central plate.

The analysis utilised the previously extracted Ogden hyper-elastic material model coefficients. The nonlinear mechanical behaviour of QZS structures is highly dependent on their geometric configuration, namely the curvatures defined by radii R1 and R2 and the initial orientation angles  $\theta1$  and  $\theta2$ . To explore this relationship, nine distinct models (SA1–SA9) were developed, with geometric parameters as described in Table 3. For this study, the radii and angles were

systematically varied (R1: 200, 100 and 50 mm, R2: 150, 100 and 80 mm,  $\theta$ 1: 15.36°, 30.71° and 61.42°,  $\theta$ 2: 17.46°, 26.18° and 32.73°) while the arch lengths of the curved beams were kept constant to isolate the effects of curvature and orientation in a fixed representative volume.

Compression analyses were performed on each configuration to determine the force-displacement response, with the results for all nine designs presented in Fig. 13. The curves display distinct characteristics, including initial buckling force, snap-through behaviour, and overall force trend. These features are critical design parameters for tailoring metamaterial performance in applications such as energy absorption and vibration isolation. The results demonstrate that the QZS behaviour is highly tuneable. The nine configurations are analysed in three groups based on the primary radius, R1 (SA1–SA3: 200 mm, SA4–SA6: 100 mm, SA7–SA9: 50 mm).

- Effects of R1: Comparing across the groups, decreasing the primary radius R1 lowers the force threshold for buckling and modifies the snap-through displacement range. For example, the buckling initiation shifts from ~2 mm of displacement for the SA1–SA3 and SA7–SA9 groups to ~4 mm for the SA4–SA6 group, while the snapthrough region spans approximately 6–10 mm for SA1–SA3, 8–12 mm for SA4–SA6, and 4–8 mm for SA7–SA9.
- Effects of R2: Within each group, decreasing the secondary radius R2 (thereby increasing the beam's curvature) consistently lowers the buckling force and extends the QZS plateau. For instance, in the first group (SA1–SA3), reducing R2 decreases the buckling force from 2.2 N to 1.5 N and extends the displacement range of the QZS region from approximately 4 mm to 8 mm. This enhances the negative stiffness as a direct result of the increased initial curvature.

These findings highlight the significant and predictable control that geometric parameters **R1** and **R2** exert over the mechanical response. Among the designs, the SA1 model provides a valuable baseline, exhibiting a clear buckling peak and a moderate QZS region suitable for comparative laboratory analyses.

FEM parametric analysis identified the SA1 model with optimal QZS characteristics for experimental validation. Consequently, TPU-based metamaterial composites were fabricated via printing according to the SA1 model. The meta-bio-composites were tested under a monotonic compression and simulated computationally, see Fig. 14. The Ogden hyper-elastic model calibrated by data in Section 3 was implemented in the FEM to replicate experimental behaviours of meta-structures.

Fig. 15a shows a comparison between experimental and computational force-displacement responses for a meta-structure made from

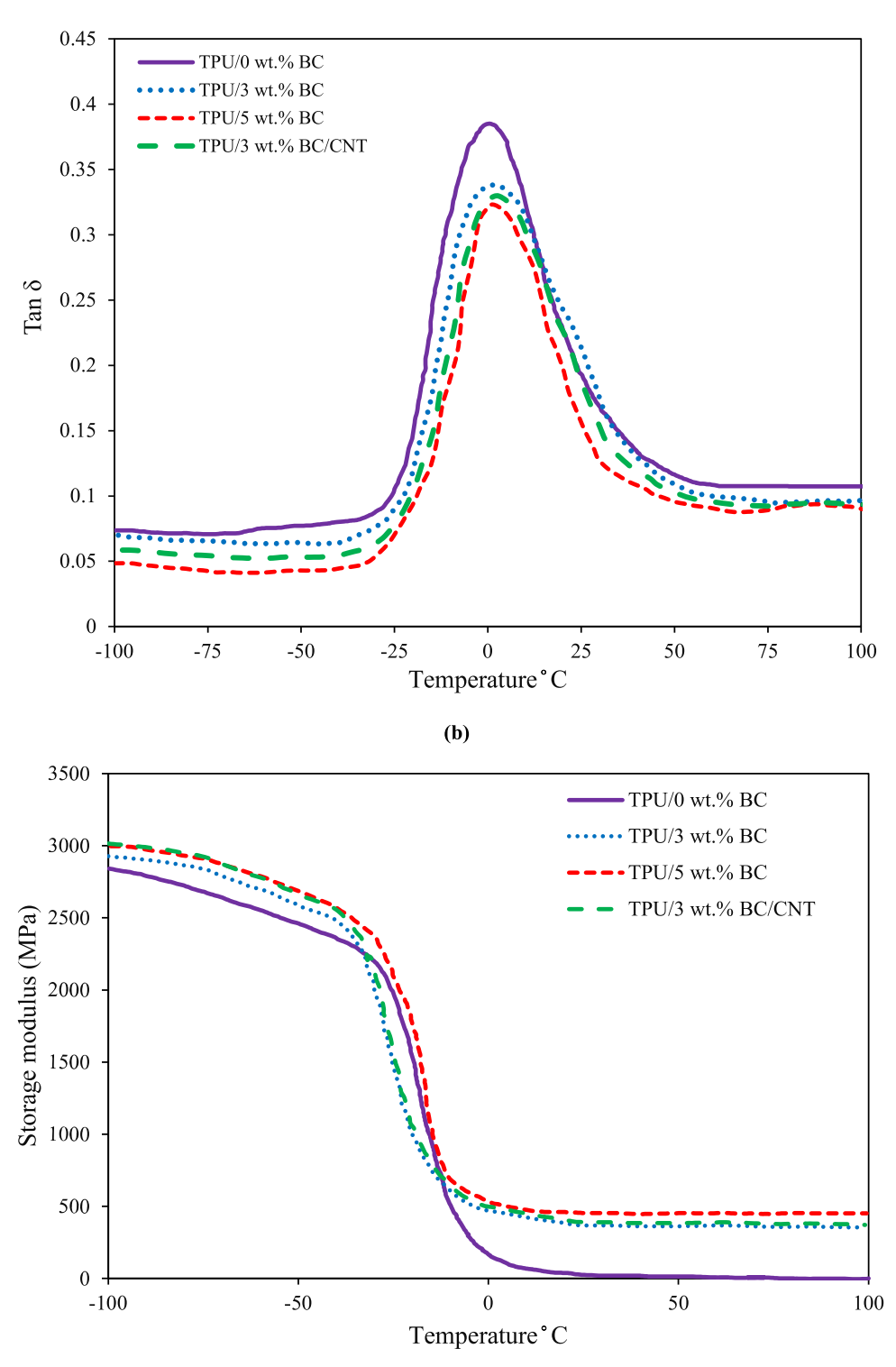


Fig. 9. DMTA results of TPU and TPU bio-composites: (a) storage modulus, (b)  $\tan \delta$ .

pure TPU. The resulting force-displacement curve shows a typical nonlinear stiffness behaviour. A nearly flat region in the curve, between about 3 mm and 9 mm of displacement, is labelled as the "QZS region". In this zone shaped like a plateau, the force remains almost constant at around 2.3 N while the displacement increases. The force shows little variation around  $\sim\!2.3$  N in the QZS region, demonstrating a negligible force required for a significant deformation. This behaviour is a key feature of QZS and is important for effective force regulation, overload

protection, and energy dissipation. Furthermore, the force-displacement response from FEM aligns well with the experimental one along the entire displacement range. FEM satisfactorily captures the initial increase in force with displacement, the near-constant force plateau in the QZS region, and the subsequent stiffening/hardening behaviour at larger displacements. Moreover, the mode shapes of the proposed QZS metamaterial were examined through both experimental and numerical analyses. Fig. 15b illustrates the mode shapes obtained from the

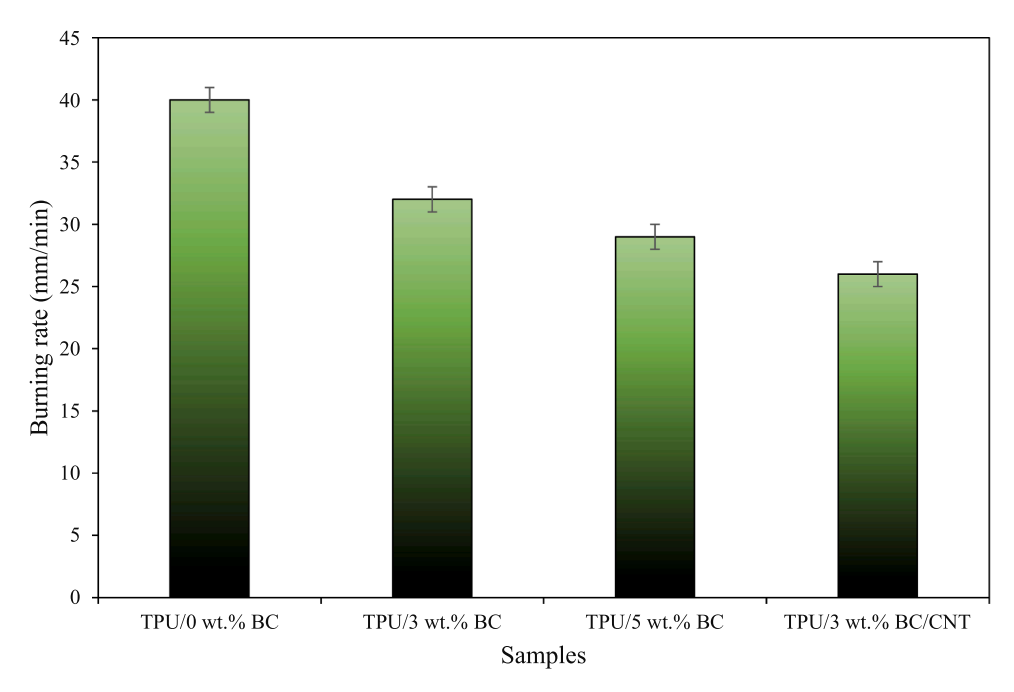


Fig. 10. Burning rate for TPU-based composites.

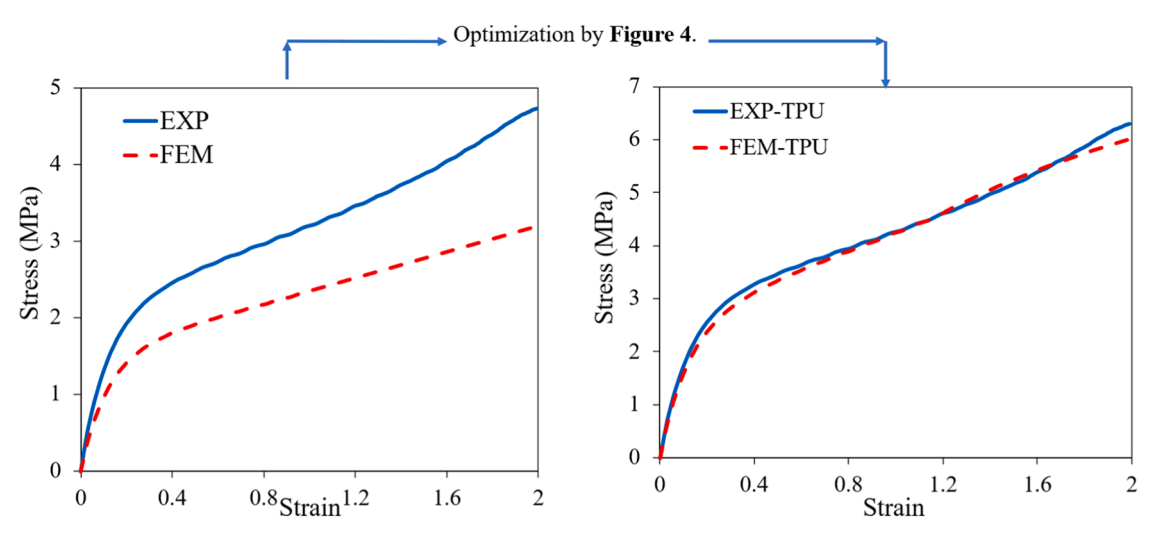


Fig. 11. Correlation between the FEM and experimental results for TPU under tensile loading.

**Table 2**Optimised parameters of the second Ogden hyper-elastic model for different biocomposites.

Samples	$\mu_1~(\mathit{MPa})$	$\alpha_1$	$\mu_2(\mathit{MPa})$	$\alpha_2$
TPU/0 wt. % BC	-0.3652	2.8105	4.5107	-4.1216
TPU/3 wt. % BC	0.2123	4.5108	3.6589	-3.0105
TPU/5 wt. % BC	0.4221	2.7881	4.8814	-2.0115
TPU/3 wt. % BC/CNT	0.6875	5.2154	4.0587	-3.6143

experiment and FEM. The metamaterial configurations predicted by FEM are close to experimental observations. Finally, the good correlation between experimental and numerical results presented in Fig. 15 corroborates that the calibrated FEM can replicate the mechanical behaviours at the structural scale.

Fig. 16 presents experimental and numerical force-displacement graphs for a QZS meta-structure 3D printed by pure TPU, TPU reinforced with 3 wt. % BC, and TPU reinforced with 3 wt. % BC and CNT. It is

seen that reinforcing TPU with BC and BC/CNT makes the TPU composite stiffer and affects the force level as well as the QZS range. The incorporation of 3wt % BC (TPU/3 wt. % BC) results in a 73 % increase in the force level across the entire displacement range compared to pure TPU. The plateau region, while still present, occurs at a higher force value ( $\sim 3.4$  N), suggesting an increase in the overall stiffness of the QZS meta-structure. The hybrid reinforcement with 3wt % BC and CNT (TPU/3 wt. % BC/CNT) leads to a further significant increase in the force level to 122 %. The QZS region, observed between approximately 3 mm and 9 mm, occurs at the highest force value ( $\sim 5.12$  N) for TPU/3 wt. % BC/CNT. The computational response for TPU, TPU/3 wt. % BC, and TPU/3 wt. % BC/CNT demonstrates a good correlation with the experimental data, indicating that the Ogden model can capture the effect of BC and CNT reinforcement on the structural output and the QZS behaviours.

To evaluate their force-displacement and energy dissipation characteristics, the QZS behaviours were further investigated under loading-unloading conditions through experimental and numerical approaches.

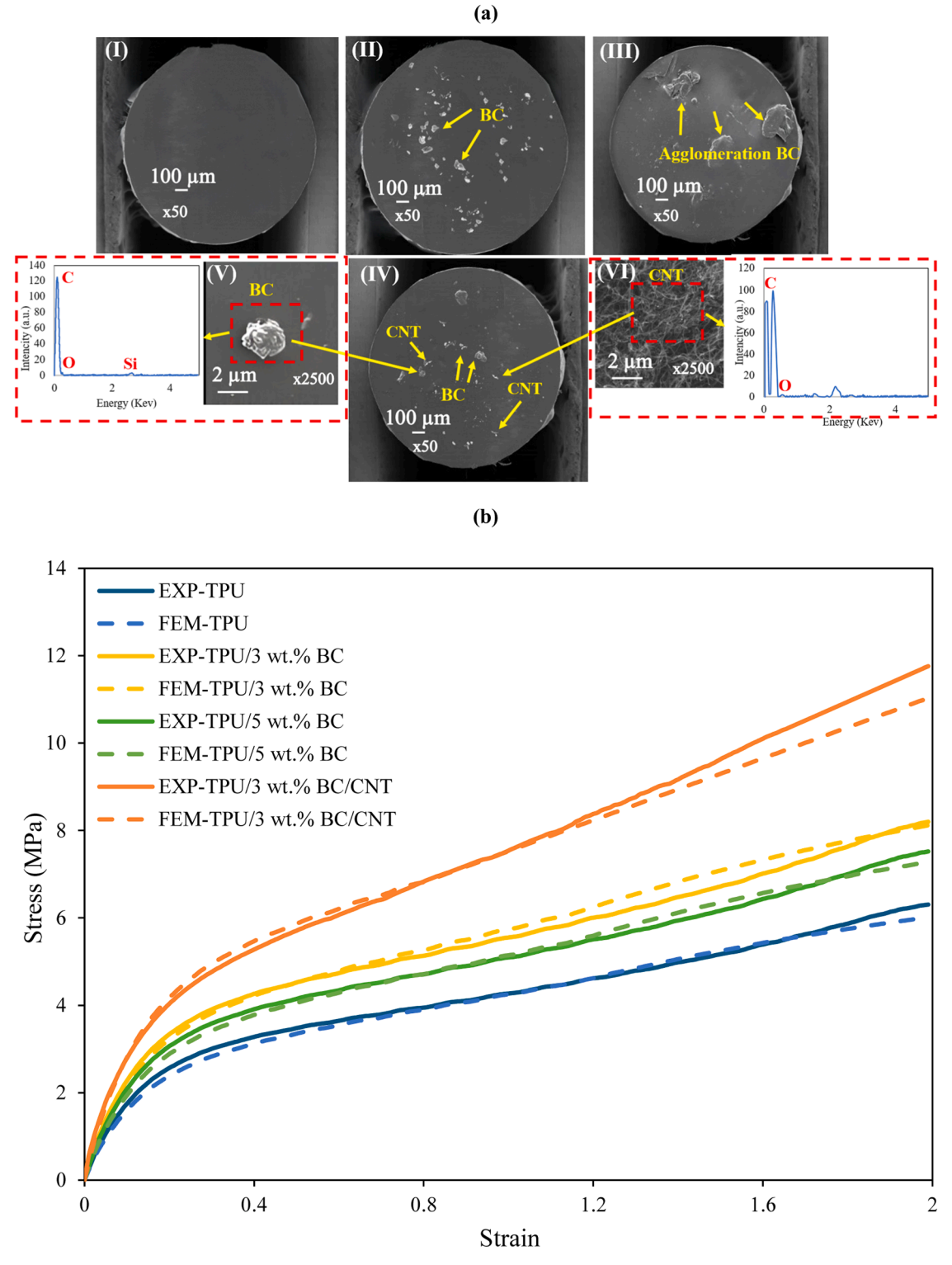


Fig. 12. (a) SEM images of the microstructure of cross section of filaments composite corresponds to (I) the pure TPU, (II) the TPU/3 wt. % BC bio-composite, (III) the TPU/5 wt. % BC bio-composite (IV) the TPU/3 wt. % BC/CNT bio-composite, (V) and (VI) higher magnifications and EDX of BC and CNT, respectively, (b) computational and experimental stress-strain response of bio-composites under monotonic tension.

Fig. 17a presents the cyclic force-displacement responses of the metamaterial systems with different compositions. It is worth noting that the hysteresis loops seen during the loading-unloading cycle reflect the material's ability to dissipate energy. The energy dissipation is mainly due to the buckling-type mechanical instability through compression with a very minor effect from the visco-elasticity. Specific energy dissipation values were calculated as 1.6 J/kg for TPU/3 wt. % BC/CNT,

1.2 J/kg for TPU/3 wt. % BC, and 0.85J/kg for pure TPU. These results demonstrate that adding 3 wt. % BC increases specific energy dissipation around 33 % compared to pure TPU and further adding 1 wt. % CNT boosts this enhancement to 88 %. A wider hysteresis loop is observed in the CNT-reinforced sample confirming its capability to dissipate a higher level of energy during loading and unloading. 1 wt. % CNT helps distribute the applied load more effectively throughout the material and

 Table 3

 Variations in geometric parameters for nine unit-cells models.

Label	$R_1$ $(mm)$	$\theta_1$	$\sim V_1 \left( mm^3  ight)$	$R_2$ $(mm)$	$\theta_2$	$\sim V_2(mm^3)$
SA1	200	15.36 °	1712	150	17.46 °	1462
SA2	200	15.36 °	1712	100	26.18 °	1462
SA3	200	15.36 °	1712	80	32.73 °	1462
SA4	100	30.71 °	1712	150	17.46 °	1462
SA5	100	30.71 °	1712	100	26.18 °	1462
SA6	100	30.71 °	1712	80	32.73 °	1462
SA7	50	61.42 °	1712	150	17.46 °	1462
SA8	50	61.42 °	1712	100	26.18 °	1462
SA9	50	61.42 °	1712	80	32.73 °	1462

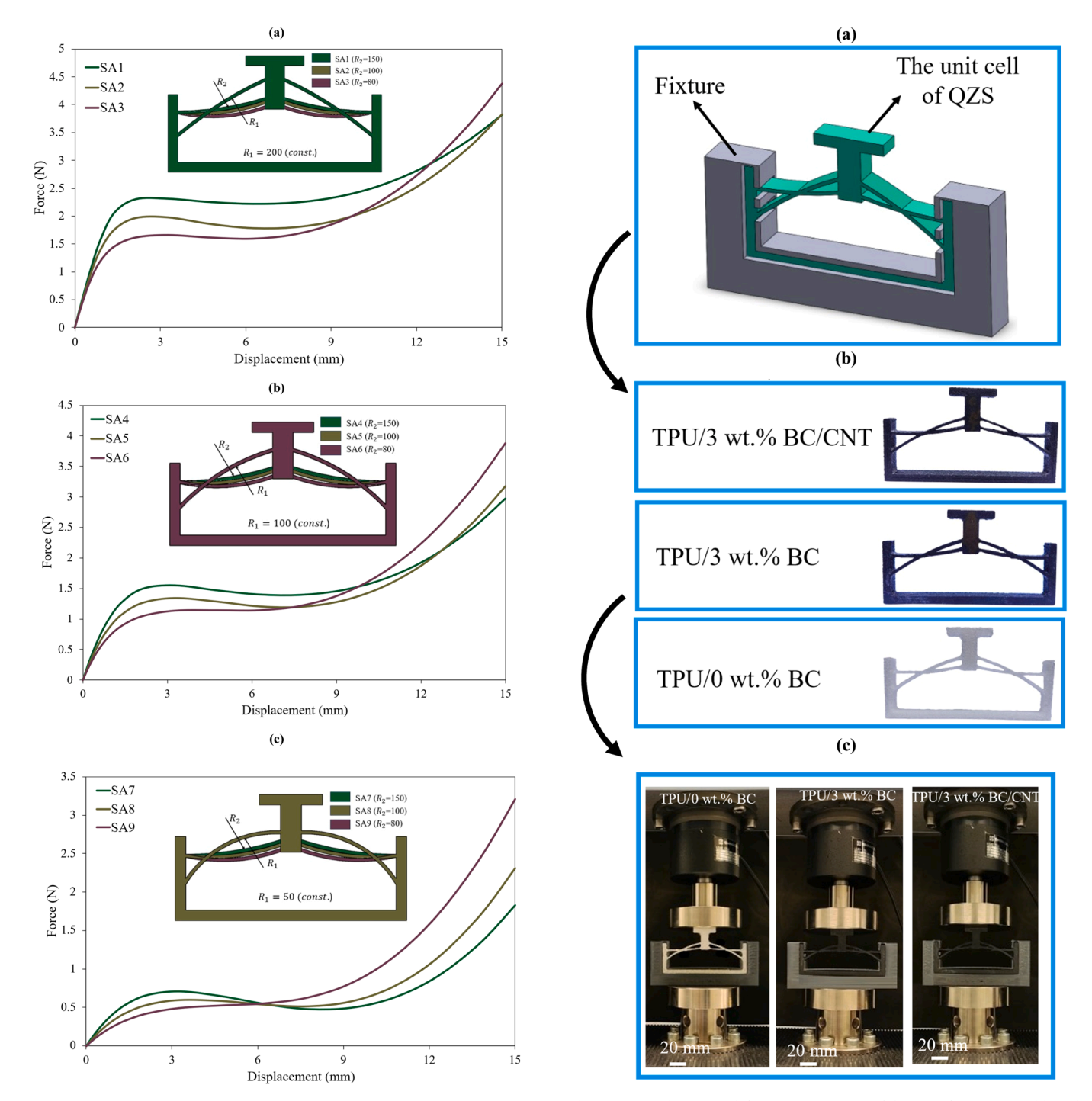
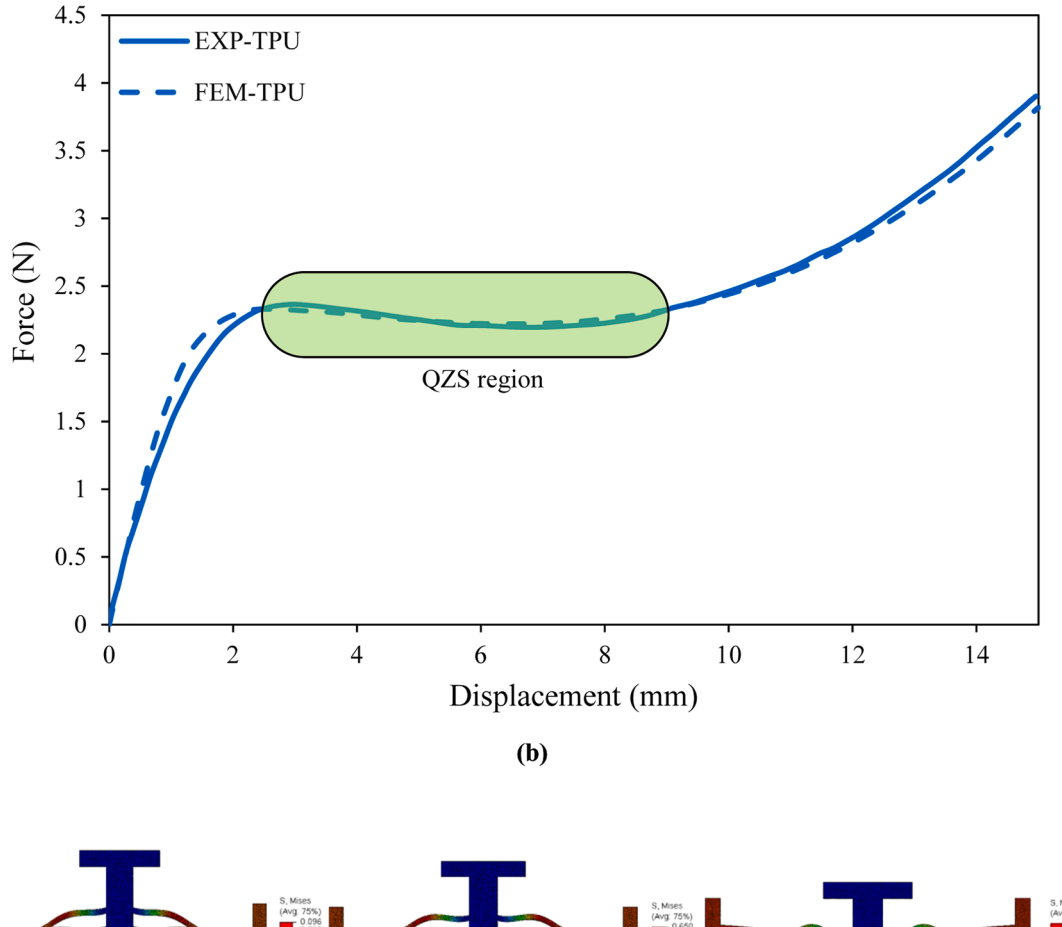


Fig. 13. Influence of geometric parameters on the force-displacement behaviour  $(a,\,b,\,c)$ .

**Fig. 14.** (a) Schematic of the QZS structure and fixture, (b) 3D-printed based composites samples, (c) uniaxial compression test setup.





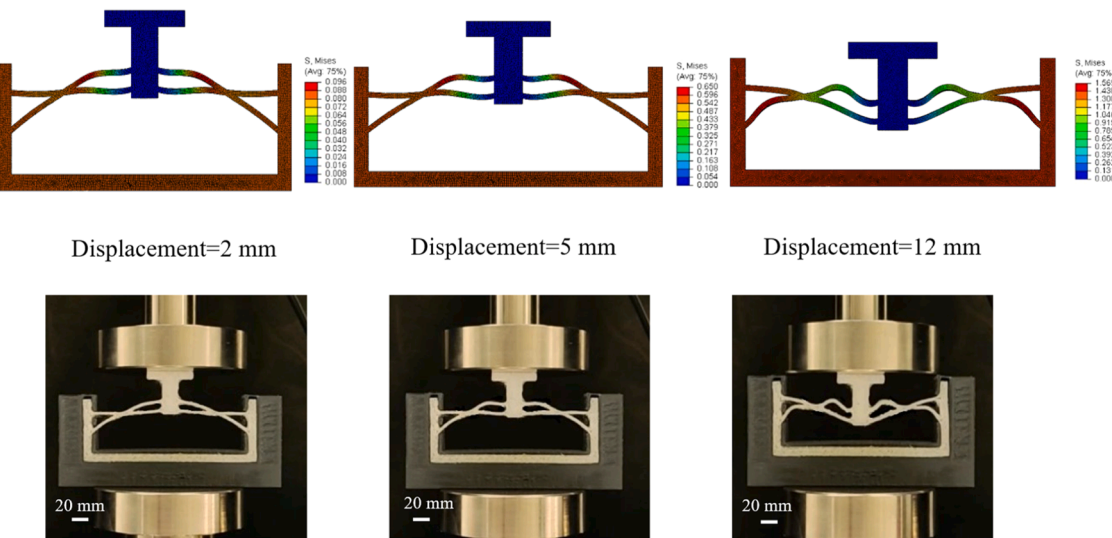


Fig. 15. Experimental and FEM analysis of TPU meta-structure under compression: (a) force-displacement response, (b) structure configuration during loading.

improves bonding between the layers and particles in the composite. Large surface area of CNT allows better interaction with the TPU matrix, leading to a stronger and more stable structure. It should be finally mentioned that the current metamaterial was designed and studied under quasi-static loading-unloading conditions. For dynamic conditions, materials damping effect should be measured and their effects should be applied to all steps from design to simulation, but they are beyond the scope of this research. Future studies could be carried out to quantitatively evaluate damping characteristics (e.g., damping ratio or loss factor) through vibration and dynamic mechanical tests.

To study the long-term durability, the TPU/3 wt. % BC sample was subjected to 1000 loading-unloading cycles. Fig. 17b shows the cyclic force-displacement response of the TPU/3 wt. % BC meta-structure. It is seen that the structures experience a drop at the upper and lower quasi constant-force plateau levels while the hysteresis loop area becomes narrower throughout the cycles. While a major drop at plateau force level and hysteresis area happens in the first 10 cycles, it becomes minor after that, and a high level of stability/overlap can be seen after 500 cycles. It is also found that the structure can retain 98 % of the maximum compressive force after 1000 cycles. It shows clear evidence of

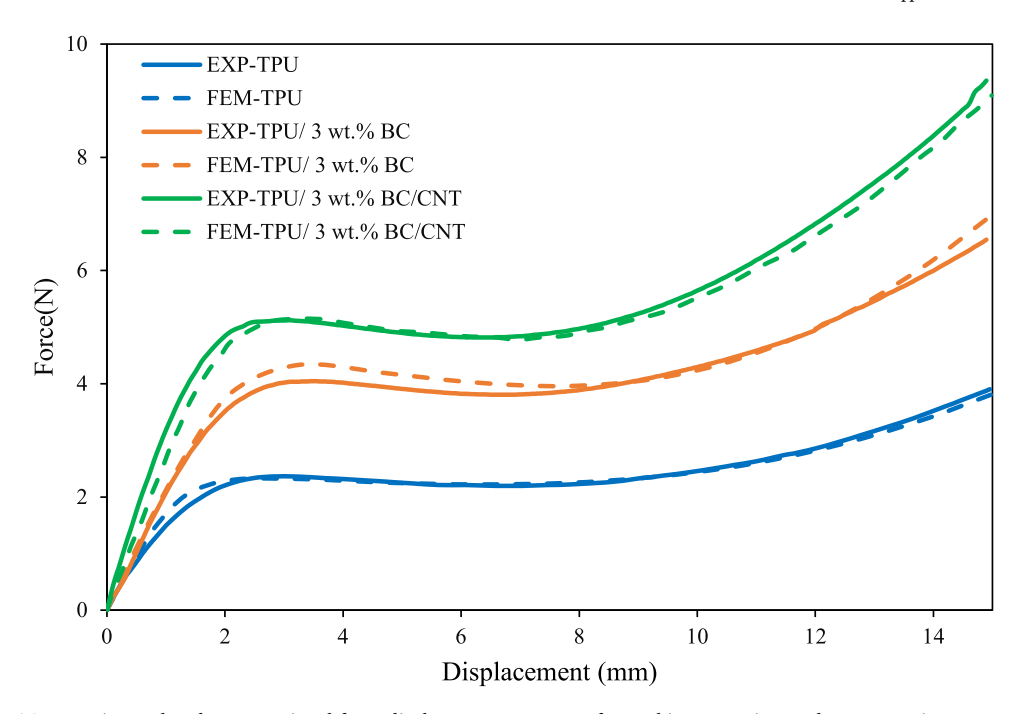


Fig. 16. Experimental and computational force-displacement response of meta-bio-composites under monotonic compression.

outstanding cyclic force durability. No residual deformation is also seen after each loading-unloading cycle as the unloading curve goes fully back to the origin. Only a small Mullins-type softening is observed predominantly within the first 10 cycles; thereafter the response stabilises with 98 % force retention by 1000 cycles. They imply that the meta-structure under repeated loading-unloading remains resilient and hyper-elastic and possesses an acceptable constant-force performance.

Fig. 18a shows a schematic of a triple-unit (multi-unit) OZS metastructure formed by circular unit cells. Also, Fig. 18b presents a finite element-based comparative analysis of the mechanical behaviour between a single-unit and a triple-unit (multi-unit) QZS meta-structure, both fabricated using pure TPU. The simulations examine the structural response under quasi-static compression, focusing on the evolution of force-displacement characteristics and internal stress distribution. Both configurations exhibit the characteristic step-wise force-displacement behaviour of QZS systems-comprising an initial region of increasing stiffness, a pronounced plateau corresponding to the QZS region, and a final stiffening phase at higher displacements. The tripleunit system preserves the QZS plateau observed in the single-unit design (2-9 mm displacement range) but supports a significantly higher constant-force response of approximately 6.9 N, compared to 2.3 N for the single unit. This threefold increase in load capacity is a direct consequence of the modular parallel configuration. The deformation is uniformly distributed across the unit cells, and the nonlinear response is consistently replicated, confirming the scalability and modularity of the design. Stress contour plots included in the figure show that internal stress distribution remains stable and spatially consistent across the multi-unit configuration. The similarity in stress patterns between both configurations further confirms the structural repeatability and mechanical integrity under increased loading. These findings validate the effectiveness of the parallel-unit approach in scaling QZS behaviour. This modular design strategy enables tailored mechanical responses-particularly force capacity-without altering the fundamental deformation mechanisms. Such adaptability is especially valuable in applications demanding programmable energy absorption or constantforce performance, including soft robotics, adaptive suspensions, and impact mitigation systems.

#### 6. Potential applications

The bio-based TPU/BC/CNT QZS metamaterial exhibits an excellent combination of modularity, scalability, tunability, and multifunctionality (e.g., flame retardancy), making it ideal for a range of sectors including robotics, automotive, and furniture, see Fig. 19. Its QZS architecture delivers large deformations under near-constant force. It enables efficient mechanical response, energy dissipation, overload protection, and force regulation. Also, some simple conceptual designs were 3D printed as shown in Fig. 19. Several potential applications are discussed below.

Soft Robotics and Manipulation Systems: In soft robotics, the modular QZS architecture offers an adaptive foundation for end-effectors and grippers that must handle fragile or irregularly shaped items. The constant-force plateau enables delicate manipulation of objects like fruits, medical instruments, or electronic components without requiring complex force feedback systems. The material's tuneable stiffness allows for programmed compliance, critical for safe human-robot interaction in collaborative robotics and service robots in unstructured environments. Interestingly, the quasi-constant force range achieved in this study aligns with the typical preload forces applied by soft robotic fingers when manipulating fragile objects, indicating the potential applicability of the designed meta-structures in soft robotic grasping tasks.

Automotive Interiors and Safety Systems: The QZS metamaterial is also well-suited for automotive applications, especially in components such as seating systems, headrests, armrests, and interior panels, where both comfort and safety are essential. Its ability to dissipate energy during impacts enhances passenger protection, while the inherent flame retardancy, enhanced by CNT and BC reinforcements—ensures compliance with stringent fire safety regulations. Furthermore, the composite's light weight and mechanical customisability align with automotive lightweighting strategies, contributing to improved fuel efficiency without compromising interior softness or crash performance.

Furniture and Adaptive Construction Materials: In furniture design, particularly for applications requiring ergonomic comfort (e.g., office chairs, beds, and sofas), the QZS material offers a combination of mechanical cushioning, fatigue resistance, and thermal stability. Its QZS behaviour protects against overloading, reduces vibrations, and improves overall sitting or resting comfort. For construction and

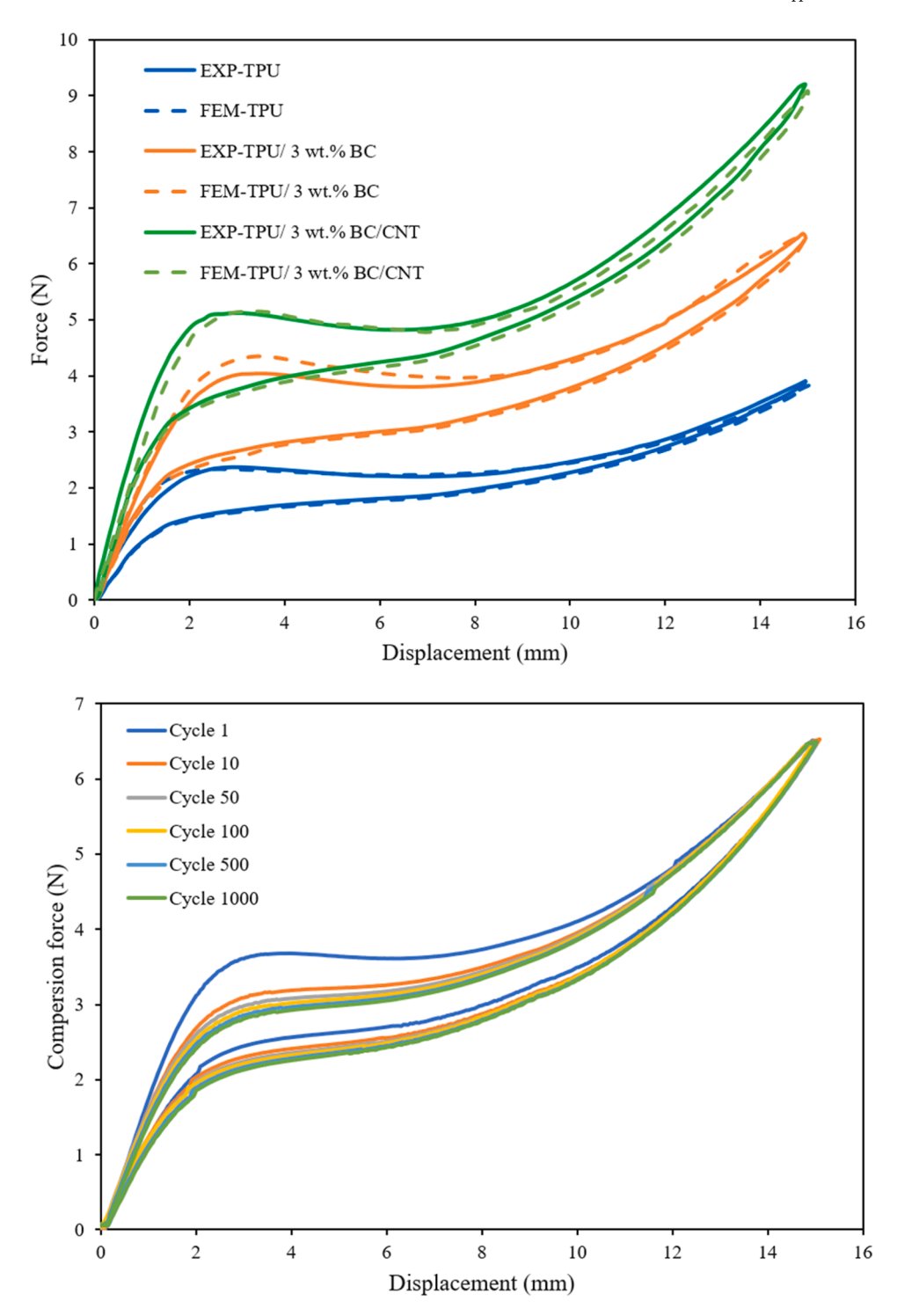


Fig. 17. (a) Experimental and computational force-displacement response of meta-bio-composites under loading-unloading cycles, (b) experimental force-displacement response of TPU/3 wt. % BC under 1000 loading-unloading cycles.

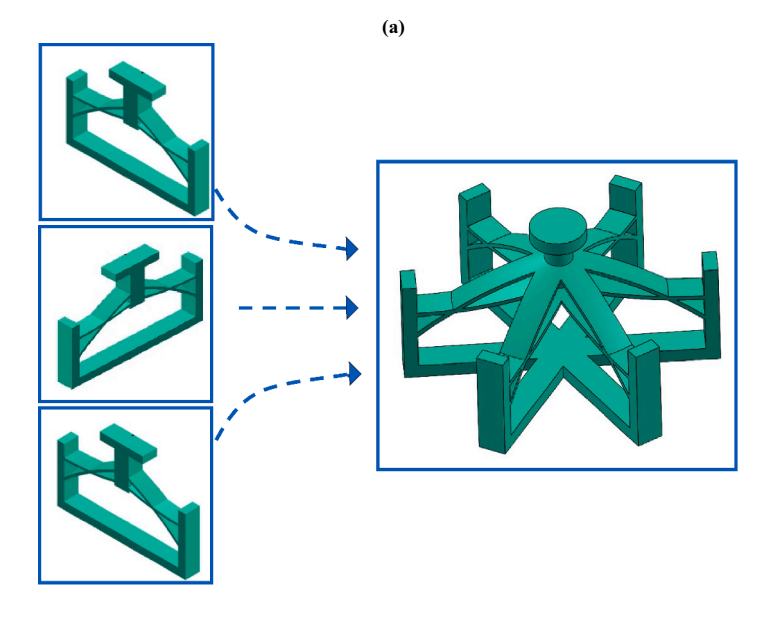
architectural applications, modular QZS components could be integrated into energy dissipating floor systems, safety padding in smart environments, or sustainable building insulation systems, where structural adaptability and passive impact protection are desired.

By merging sustainability, mechanical programmability, and multifunctionality, the TPU/BC/CNT-based QZS metamaterial represents a versatile platform for next-generation systems that demand softness, protection, and environmental responsibility, all in one. Its scalability and customisability make it ideal not just for isolated applications, but also as a core component of future smart, responsive, and sustainable

product ecosystems.

# 7. Conclusion

This study developed a novel bio-composite QZS metamaterial by integrating material design, hyper-elastic constitutive modelling, structural conceptual design, and finite element modelling in a unified framework. Reinforcing bio-based TPU with 3 wt. % bamboo charcoal and 1 wt. % carbon nanotubes not only enhanced its tensile strength and flame resistance, but also enabled 3D printing of highly stable, tuneable



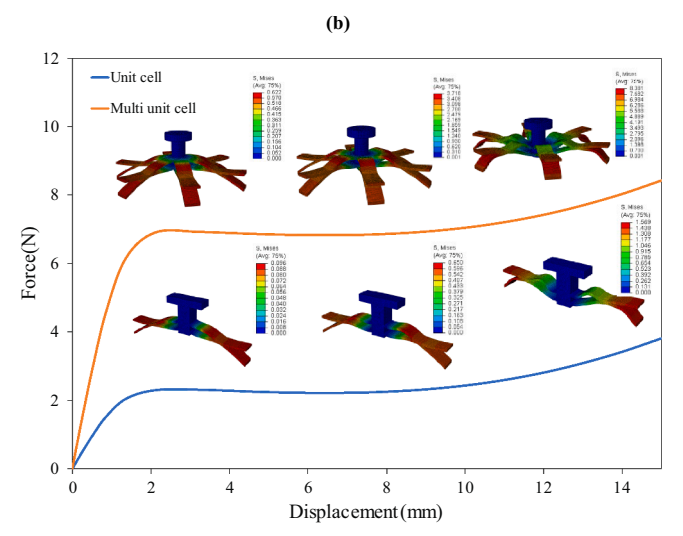


Fig. 18. (a) Schematic of a triple-unit (multi-unit) QZS meta-structure formed by circular unit cells, (b) FEM-based analysis of force-displacement response in single and multi-unit QZS meta-structures.

QZS meta-structures. The proposed surrogate-based Ogden model successfully bridged experimental data with predictive FEM simulations, guiding the design of ribcage-inspired metamaterials that exhibited a stable constant-force plateau and strong energy dissipation under repeated loading-unloading. The main conclusions are summarised as follows:

- 1. *Mechanical enhancement:* Reinforcing TPU with 3wt % BC and 1wt % CNT increased the material tensile strength by 86 % and improved specific energy dissipation of meta-structures by 88 %, demonstrating superior mechanical performance.
- 2. *Fire retardancy:* Flame retardancy was enhanced, with the addition of 3 wt. % BC and 1 wt. % CNT reducing the burning rate by 35 %.
- 3. Durability under cyclic loading: Loading-unloading compression tests showed stable force-displacement responses with a small Mullinstype softening concentrated in the first 10 cycles and 98 % maximum-force retention by 1000 cycles, confirming long-term structural integrity and consistency.
- Model validation: Finite element simulations using the hyper-elastic Ogden material model closely matched experimental behaviour,

- validating the numerical modelling accuracy and surrogate-based material parameter identification.
- Metamaterial design: Mechanical metamaterial design leads to a plateau region of 6 mm with a tuneable constant-force response ranging from 2.3 to 5.12 N, tailored for QZS performance.
- Scalability: A modular triple-unit cell design tripled the force output while preserving the QZS characteristics without performance loss, proving the scalability of the conceptual design.
- 3D printability: Melt flow index analysis confirmed that the composites remain extrudable and 3D printable, supporting practical FFF printing.

These multifunctional, scalable metamaterials offer significant potential for diverse real-world applications where controlled force transmission, compliance, and safety are paramount. Their bio-inspired architecture, tuneable mechanical behaviour, and flame-retardant performance make them ideal for integration in soft robotics, prosthetic and orthotic interfaces, automotive interiors, wearable medical devices, and impact mitigation systems. The proposed TPU/BC/CNT QZS metamaterials thus present a sustainable, adaptive platform for next-generation meta-structures in robotics, healthcare, automotive

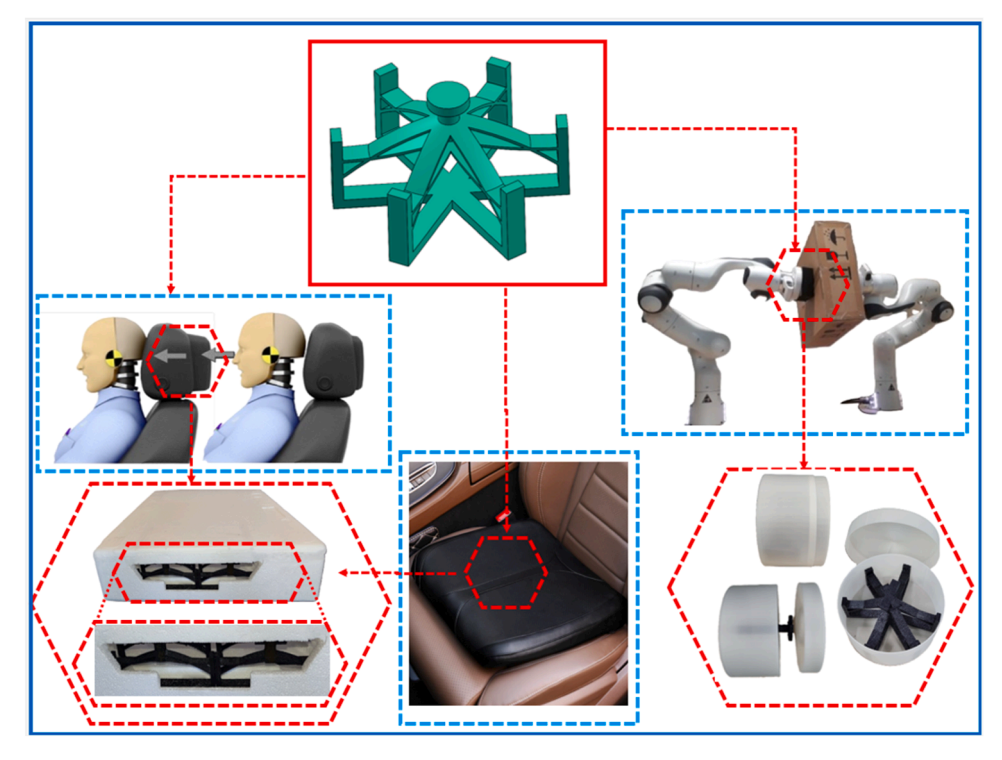


Fig. 19. Illustration of potential application domains for the proposed QZS metamaterials, including automotive, soft robotics, furniture, and adaptive construction materials.

systems, interior design and beyond.

#### CRediT authorship contribution statement

K. Rahmani: Writing – review & editing, Writing – original draft, Visualization, Validation, Software, Methodology, Investigation, Formal analysis, Data curation, Conceptualization. H. Malekmohammadi: Writing – review & editing, Writing – original draft, Methodology, Investigation, Data curation. A.M. Haque: Writing – review & editing, Supervision, Methodology, Investigation. S. Karmel: Writing – review & editing, Supervision, Methodology, Investigation. C. Branfoot: Writing – review & editing, Supervision, Methodology, Investigation. I. Pande: Writing – review & editing, Supervision, Methodology, Investigation. P. Breedon: Writing – review & editing, Supervision, Methodology, Investigation. M. Bodaghi: Writing – review & editing, Writing – original draft, Validation, Supervision, Resources, Project administration, Methodology, Investigation, Funding acquisition, Data curation, Conceptualization.

# **Declaration of competing interest**

The authors declare that they have no known competing financial interests or personal relationships that could have appeared to influence the work reported in this paper.

# Acknowledgements

The authors gratefully acknowledge the support by the Engineering and Physical Sciences Research Council (EPSRC) [I5M project, award number: EP/Y011457/1], and the EPSRC's Innovation Launchpad Network+ Researcher in Residence scheme [BIO-CYCLE project, grant numbers: EP/W037009/1, EP/X528493/1, award number: RIR26C230615–6, Researcher: Mahdi Bodaghi].

# Data availability

Data will be made available on request.

#### References

- L. Du, et al., Mechanically programmable composite metamaterials with switchable positive/negative Poisson's ratio, Adv. Funct. Mater. 34 (22) (2024) 2314123.
- [2] E.B. Duoss, et al., Three-dimensional printing of elastomeric, cellular architectures with negative stiffness, Adv. Funct. Mater. 24 (31) (2014) 4905–4913.
- [3] G. Wang, et al., A novel 3D topological metamaterial for controllability of polarization-dependent multilayer elastic waves, Compos. Part B: Eng. 275 (2024) 11124
- [4] S. Guo, S. Liu, R. Gao, A bidirectional quasi-zero stiffness metamaterial for impact attenuation, Int. J. Mech. Sci. 268 (2024) 108998.
- [5] J. Yi, et al., Stability-enhanced variable stiffness metamaterial with controllable force-transferring path, Adv. Funct. Mater. 35 (4) (2025) 2413789.
- [6] C. Zhou, et al., A nonlinear low frequency quasi zero stiffness vibration isolator using double-arc flexible beams, Int. J. Mech. Sci. 276 (2024) 109378.
- [7] C. Zeng, et al., Stair-stepping mechanical metamaterials with programmable load plateaus, Adv. Funct. Mater. 34 (49) (2024) 2408887.
- [8] B.R. Krishnan, et al., Auxetic structure metamaterial for crash safety of sports helmet, Mater. Today: Proceed. 56 (2022) 1043–1049.
- [9] C. Cai, et al., Design and numerical validation of quasi-zero-stiffness metamaterials for very low-frequency band gaps, Compos. Struct. 236 (2020) 111862.
- [10] S. Dalela, et al., Nonlinear static and dynamic response of a metastructure exhibiting quasi-zero-stiffness characteristics for vibration control: an experimental validation, Sci. Rep. 14 (1) (2024) 19195.
- [11] A. Carrella, et al., On the force transmissibility of a vibration isolator with quasizero-stiffness, J. Sound. Vib. 322 (4–5) (2009) 707–717.
- [12] J. He, et al., Quasi-zero stiffness metamaterials with programmable multistability for multi-scenario applications, Appl. Mater. Today 46 (2025) 102864.
- [13] X. Sun, Z. Qi, J. Xu, Vibration properties of a knee bio-inspired nonlinear isolation structure, Int. J. Non. Linear. Mech. 147 (2022) 104245.
- [14] W. Liu, et al., Origami-inspired quasi-zero stiffness metamaterials for low-frequency multi-direction vibration isolation, Appl. Phys. Lett. (8) (2023) 123.
- [15] R. Hamzehei, M. Bodaghi, N. Wu, Mastering the art of designing mechanical metamaterials with quasi-zero stiffness for passive vibration isolation: a review, Smart Mater. Struct. 33 (8) (2024) 083001.
- [16] J. Ji, Q. Luo, K. Ye, Vibration control based metamaterials and origami structures: a state-of-the-art review, Mech. Syst. Signal. Process. 161 (2021) 107945.
- [17] X. Zhou, et al., 4D printed bio-inspired polygonal metamaterials with tunable mechanical properties, Thin-Walled Struct. 205 (2024) 112609.
- [18] M. Bodaghi, W.H. Liao, 4D printed tunable mechanical metamaterials with shape memory operations, Smart Mater. Struct. 28 (4) (2019) 045019.

- [19] M.J. Islam, B. Bao, F. Peng, Recent developments of mechanical metamaterials inspired by origami: from methodologies, fabrication to challenges, Appl. Mater. Today 44 (2025) 102715.
- [20] S. Ravanbod, et al., From coral to control: bio-inspired, 3D-printable metamaterials with tuneable quasi-zero stiffness and multi-functional bio-composites, Mater. Des. (2025) 114398.
- [21] Y. Lu, Q. Luo, L. Tong, Topology optimization for metastructures with quasi-zero stiffness and snap-through features, Comput. Methods Appl. Mech. Eng. 434 (2025) 117587.
- [22] Y. Xu, H.-W. Dong, Y.-S. Wang, Topology optimization of programable quasi-zerostiffness metastructures for low-frequency vibration isolation, Int. J. Mech. Sci. 280 (2024) 100557
- [23] H. Wang, et al., A review on the mechanical metamaterials and their applications in the field of biomedical engineering, Front. Mater. 10 (2023) 1273961.
- [24] D. Rigotti, A. Dorigato, A. Pegoretti, Multifunctional 3D-printed thermoplastic polyurethane (TPU)/multiwalled carbon nanotube (MWCNT) nanocomposites for thermal management applications, Appl. Sci. 14 (20) (2024) 9614.
- [25] U. Khan, et al., Tuning the mechanical properties of composites from elastomeric to rigid thermoplastic by controlled addition of carbon nanotubes, Small 7 (11) (2011) 1579–1586.
- [26] M. Bodaghi, et al., 3D/4D printed bio-composites reinforced by bamboo charcoal and continuous flax fibres for superior mechanical strength, flame retardancy and recoverability, Polym. Test. 143 (2025) 108709.
- [27] K. Rahmani, et al., Flexible bio-composites with continuous natural fibre and bamboo charcoal: enhanced flame retardancy, mechanical resilience, energyabsorbing & printability performance, Virtual. Phys. Prototyp. 20 (1) (2025) e2534845
- [28] A. Damanpack, M. Bodaghi, W. Liao, A robust hyper-elastic beam model under biaxial normal-shear loadings, Int. J. Non. Linear. Mech. 95 (2017) 287–295.

- [29] W. Liu, et al., Programmable quasi-zero-stiffness metamaterials, Engineering 47 (2025) 160–167.
- [30] L. Yang, et al., 3D Printing of carbon nanotube (CNT)/thermoplastic polyurethane (TPU) functional composites and preparation of highly sensitive, wide-range detectable, and flexible capacitive sensor dielectric layers via fused deposition modeling (FDM), Adv. Mater. Technol. 8 (7) (2023) 2201638.
- [31] H. Guo, et al., Preparation of thermoplastic polyurethane/multi-walled carbon nanotubes composite foam with high resilience performance via fused filament fabrication and CO2 foaming technique, Polymers. (Basel) 15 (6) (2023) 1535.
- [32] E.H. Twizell, R.W. Ogden, Non-linear optimization of the material constants in Ogden's stress-deformation function for incompressinle isotropic elastic materials, J. Aust. Math. Society. Series B. Appl. Math. 24 (4) (2009) 424–434.
- [33] A. Nurdina, M. Mariatti, P. Samayamutthirian, Effect of single-mineral filler and hybrid-mineral filler additives on the properties of polypropylene composites, J. Vinyl and Addit. Technol. 15 (1) (2009) 20–28.
- [34] B.A. Alshammari, et al., Impact of hybrid fillers on the properties of high density polyethylene based composites, Polymers. (Basel) 14 (16) (2022) 3427.
- [35] Y. Kanbur, U. Tayfun, Investigating mechanical, thermal, and flammability properties of thermoplastic polyurethane/carbon nanotube composites, J. Thermoplastic Compos. Mater. 31 (12) (2018) 1661–1675.
- [36] T. Kashiwagi, et al., Thermal and flammability properties of polypropylene/carbon nanotube nanocomposites, Polymer. (Guildf) 45 (12) (2004) 4227–4239.
- [37] A. Lewandowski, K. Wilczyński, Modeling of twin screw extrusion of polymeric materials, Polymers. (Basel) 14 (2) (2022) 274.
- [38] J. Zhu, J. Jia, S.C. Tjong, Preparation, structure, and application of carbon nanotubes/bamboo charcoal composite. Nanocrystalline Materials, Elsevier, 2014, pp. 1–25.